Abstract

Gene therapy of ALS with RNA interference

Takanori Yokota, M.D.

Department of Neurology and Neurological Science, Tokyo Medical and Dental University

RNA interference (RNAi) is the process of sequence-specific, post-tanscriptional gene silencing, initiated by double-stranded RNA (dsRNA). The gene therapy for familial ALS with siRNA had been started and showed promising results in the model mouse. There is a recent progress in the delivery of siRNA to the central nervous system. There are still important problems for application of gene therapy including off-target effect and gene delivery of siRNA, but a rapid progress can be expected because of the extremely high efficiency of siRNA.

(Clin Neurol, 49: 821—823, 2009)

Key words: small-interfering RNA, short-hairpin RNA, AAV, gene therapy, RNA interference

＜シンポジウム3＞中枢神経系の再生・次なる半世紀

オーバービュー

座長　慶應義塾大学医学部生理学教室　岡野　栄之
東京医科歯科大学大学院医歯学総合研究科脳神経病態学分野　水澤　英洋

（臨床神経，49：824，2009）

現在中枢神経系の再生はもっともホットな研究領域になりつつある．本シンポジウムでは，中枢神経系の再生の研究を進めておられる最先端の研究者の皆様にup dataした研究成果を発表いただき，次の半世紀の中枢神経系の再生戦略を議論した．岡野　栄之（慶大）は「iPS細胞技術と神経疾患研究」について講演し，人工多能性幹細胞（iPS細胞）をもちいた中枢神経系の再生戦略ならびに疾患モデル研究としての有用性を示した．木山　博資（大阪市大）は，「遺伝子導入による損傷神経の温存再生促進―その治療標的の多様性―」について講演し，中枢神経損傷後の神経細胞の変性を最小限にとどめ，中枢神経が潜在的に有する再生能を引き出すために，神経細胞の生存メカニズムや軸索再生促進の分子メカニズムを解析した．そこでえられた再生関連遺伝子を導入し，機能修復をおこなう試みについて紹介した．近年，成人の脳にも幹細胞が存在しニューロンが継続的に産生されていることが明らかになったが，澤本　和延（名古屋市大）は，「脳に内在する神経再生機構」について講演した．成熟した脳におけるニューロンの産生は，霊長類をふくむ様々な動物の側脳室の脳室下帯で観察されている．脳室下帯で生まれるニューロンは長距離を移動して成熟する．動物実験で明らかになった正常時・病態時におけるニューロンの産生・移動・成熟のメカニズムと，それを活かした虚血性脳疾患の再生医療の可能性について述べた．最後に高橋　淳（京都大学）は「細胞移植による神経再生の将来」について講演し，パーキンソン病を例にとって細胞移植治療の現状と展望を考察した．胎児黒質細胞移植はすでに400例以上臨床応用されており，60歳以下の中・軽症例では症状改善が報告されている．しかし移植後の不随運動がみられた例があり十分な移植細胞量を確保するのも困難なため，広く普及するにはいたっておらず，幹細胞をもちいた細胞移植に期待が寄せられている．ラットやカニクイザルモデルではES細胞由来ドーパミン産生神経前駆細胞の移植により症状改善が報告されている．ヒトES細胞やヒトiPS細胞からもドーパミン産生神経の分化誘導が報告されており，これらの細胞をもちいた臨床応用が期待され，そのためには，腫瘍形成抑制のための未分化細胞排除技術や動物由来因子をもちいない分化誘導技術の開発が必要であることを示した．

（受付日：2009年5月21日）

FEBS Letters 583 (2009) 213–218

FEBS Letters

journal homepage: www.FEBSLetters.org

Silencing efficiency differs among tissues and endogenous microRNA pathway is preserved in short hairpin RNA transgenic mice

Hiroki Sasaguri [a,c], Tasuku Mitani [b], Masayuki Anzai [b], Takayuki Kubodera [a,c], Yuki Saito [a], Hiromi Yamada [a], Hidehiro Mizusawa [a,c], Takanori Yokota [a,*]

[a] Department of Neurology and Neurological Science, Graduate School, Tokyo Medical and Dental University, 1-5-45 Yushima, Bunkyo-ku, Tokyo 113-8519, Japan
[b] Institute of Advanced Technology, Kinki University, 14-1 Minami-Akasaka, Kainan, Wakayama 642-0017, Japan
[c] Twenty-First Century Center of Excellence Program on Brain Integration and Its Disorders, Tokyo Medical and Dental University, 1-5-45 Yushima, Bunkyo-ku, Tokyo 113-8519, Japan

ARTICLE INFO

Article history:
Received 28 August 2008
Revised 20 November 2008
Accepted 1 December 2008
Available online 11 December 2008

Edited by Ulrike Kutay

Keywords:
RNA interference
Short hairpin RNA
Small interfering RNA
Transgenic mice
MicroRNA
Oversaturation

ABSTRACT

In short hairpin RNA (shRNA) transgenic mice, the tissue difference in gene silencing efficiency and oversaturation of microRNA (miRNA) pathway have not been well assessed. We studied these problems in our previously-reported anti-copper/zinc superoxide dismutase (SOD1) shRNA transgenic mice. Although there was a tissue difference (liver and skeletal muscle, >95%; central nervous system and lung, ~80%), the target gene silencing was systemic and our anti-SOD1 shRNA transgenic mice recapitulated the SOD1-null mice. Neither endogenous miRNAs nor their target gene levels were altered, indicating the preservation of endogenous miRNA pathways. We think that the shRNA transgenic mice can be utilized for gene analysis.

1. Introduction

RNA interference (RNAi) is evolutionally conserved sequence-specific post-transcriptional gene silencing, which is mediated by small double stranded RNA (dsRNA) [1]. The long dsRNA is cleaved by an RNase III enzyme, Dicer, in cytoplasm to generate small interfering RNA (siRNA) that is 21–23 base pair dsRNA. The target mRNA is recognized by guide (antisense) strand of the dsRNA in RNA-induced silencing complex (RISC), and is cleaved by Argonaute-2 (Ago2) protein, one of the main components of RISC [2]. This post-transcriptional gene silencing can be effectively induced by exogenously introduced siRNA or intracellularly expressed short hairpin RNA (shRNA) in mammalian cells [2,3].

The shRNA transgenic mice have been published [4–7] and expected to be an alternative method to the conventional knockout mice. For using shRNA transgenic mice as a tool for gene analysis in vivo, we need to know difference in silencing efficiency among tissues. Moreover, in shRNA transgenic mice, it is also important to elucidate whether microRNA (miRNA) is normally processed, because shRNA and miRNA share intracellular machineries for their maturation in mammalian cells [8–10]. We had generated anti-mouse copper/zinc superoxide dismutase (SOD1) shRNA transgenic mice, in which shRNA was ubiquitously expressed by the RNA polymerase III (Pol III) promoter [11]. Using these mice, we here evaluated the silencing efficiency in various tissues and studied endogenous miRNA pathway.

2. Materials and methods

2.1. Generation of anti-SOD1 shRNA transgenic mice

All experiments were approved by the Animal Experiment Committees of Tokyo Medical and Dental University (#0090104) and Kinki University (KAAT-19-006). We generated an anti-SOD1

Abbreviations: shRNA, short hairpin RNA; miRNA, microRNA; RNAi, RNA interference; dsRNA, double stranded RNA; RISC, RNA-induced silencing complex; Ago2, Argonaute-2; SOD1, copper/zinc superoxide dismutase; Pol III, polymerase III; ES, embryonic stem; PBS, phosphate-buffered saline; SDS, sodium dodecyl sulfate; cDNA, complementary DNA; RT-PCR, reverse transcription polymerase chain reaction; GAPDH, glyceraldehyde-3-phosphate dehydrogenase; snRNA, small nuclear RNA; AAV, adeno-associated virus

* Corresponding author. Fax: +81 3 5803 0169.
E-mail address: tak-yokota.nuro@tmd.ac.jp (T. Yokota).

0014-5793/$34.00
doi:10.1016/j.febslet.2008.12.012

shRNA expression vector and anti-SOD1 shRNA transgenic mice as reported previously [11,12]. In brief, we inserted anti-SOD1 shRNA driven by human U6 promoter into pUC19 (Takara). The shRNA expression vector was introduced into the 129/Sv embryonic stem (ES) cells (Chemicon) by electroporation. The ES cell clones in which SOD1 protein levels were effectively suppressed were introduced into C57BL/6 blastocysts (CLEA) by microinjection. We obtained F1 transgenic mice by crossing the chimeric male mice with wild-type C57BL/6 female mice.

2.2. Histological study

To analyze hepatic lipid accumulation, liver samples from 8-month-old shRNA transgenic male mice and wild-type littermates were sectioned (4 μm) and fixed in 4% paraformaldehyde/phosphate-buffered saline (PBS) for 5 min, and then stained with filtrated Sudan III (Muto pure chemicals) at 37 °C for 30 min. Counterstaining of nuclei was performed with Mayer hematoxylin solution (Muto pure chemicals) for 3 min.

2.3. Western blot analysis

Western blot analysis was performed as reported previously [11]. Mice were killed under anesthesia with pentobarbital sodium, and perfused with cold PBS. Tissues were homogenized in the cold buffer containing 0.1% sodium dodecyl sulfate (SDS), 1% sodium deoxycholate, 1% Triton X-100, 1 mM phenylmethylsulfonyl fluoride and protease inhibitor cocktail (Sigma). Equal amounts of protein from each sample were loaded in the assays. The separated proteins were detected by specific primary antibodies; rabbit anti-SOD1 antibody (1:5000, StressGen Biotechnologies), mouse anti-β-tubulin antibody (1:1000, BD Biosciences), mouse anti-Actin antibody (1:1000, Santa Cruz Biotechnology), mouse anti-Ago2 antibody (1:500, Abcam), or rabbit anti-N-ras antibody (1:500, Santa Cruz Biotechnology).

2.4. Northern blot analysis

Northern blot analysis was performed as reported previously [11]. Ten micrograms of total RNA from each sample were loaded in the assays. The DNA probes which were used to detect RNAs were as follows; complementary DNA (cDNA) (bases 15–495) for mouse SOD1; cDNA (bases 300–614) for mouse glyceraldehyde-3-phosphate dehydrogenase (GAPDH); 5′-GGTGGAAATGAAGAAAGTAC-3′ for anti-SOD1 siRNA guide strand; 5′-ACTATACAACCTACTACCTCA-3′ for mouse let-7a; 5′-GGCATTCACCGCGTGCCTTA-3′ for mouse miR-124a; 5′-AAATATGGAACGCTTCACGA-3′ for mouse U6 small nuclear RNA (snRNA).

2.5. Quantitative reverse transcription polymerase chain reaction (RT-PCR)

After treating with TURBO DNA-free (Ambion) to remove residual genomic DNA, 1 μg of total RNA from each sample was reversely transcribed to cDNA using SuperScript III Reverse Transcriptase (Invitrogen). The cDNA was used for quantitative PCR with TaqMan system using the ABI Prism 7700 Sequence Detection System (Applied Biosystems) according to the manufacturer's protocol. The primers and probe used to quantify mouse SOD1 were 5′-GGTGCAGGGAACCATCCA-3′ for forward primer, 5′-CCCATGCTGGCCTTCAGT-3′ for reverse primer, and 5′-AGGCAAGCGGTGAACCAGTTGTGTTG-3′ for probe. The primer and probe sets of mouse GAPDH, N-ras and N-myc were purchased from Applied Biosystems. GAPDH was used to normalize the quantitative RT-PCR values.

2.6. Laser microdissection and RNA extraction from motor neurons and non-neuronal cells

Collection of motor neurons and non-neuronal cells was performed as reported previously [13]. Spinal cords of the transgenic mice or wild-type littermates were removed and embedded in Tissue-Tek O.C.T. Compound (Sakura Finetek). Seven micrometer thick sections were mounted on a MembraneSlide (Leica) and stained with HistoGene staining solution (Arcturus). Approximate one thousand motor neurons and neighboring non-neuronal cells were dissected from the ventral horn of the lumbar spinal cord for each mouse using an AS LMD system (Leica). Total RNA was extracted using RNeasy Micro Kit (Qiagen) according to the manufacturer's protocol.

2.7. Subcellular fractionation

Subcellular fractionation was performed as described previously [14]. The cerebrum or liver was gently homogenized in cold buffer (0.22 M D-mannitol, 0.07 M sucrose, at 1 mg tissue/10 μl buffer) with a glass-Teflon homogenizer (30 up-and-down strokes), and centrifuged at 600×g for 10 min. The pellets were suspended with 2.2 M sucrose and centrifuged at 40000×g for 1 h. The resulting pellets were used as nuclear fraction. The supernatants generated by the first centrifugation were used as cytoplasmic fraction. Total RNA was extracted using ISOGEN (Nippon Gene) for nuclear fraction and ISOGEN-LS (Nippon Gene) for cytoplasmic fraction, respectively.

2.8. Statistical analysis

Student's *t*-test was used to evaluate difference among tissues or difference between transgenic mice and wild-type littermates. Significance was set at $P < 0.05$. To compare the expression level on Western blot or Northern blot analysis, we used NIH ImageJ to quantify the band intensity.

3. Results

3.1. Anti-SOD1 shRNA transgenic mice recapitulate SOD1-null mice

As reported previously, we obtained anti-SOD1 shRNA transgenic mice (Fig. 1A) [11]. The silencing effect of the target gene was significant on both RNA and protein levels, and was stable with age and through to the F3 generation [11]. In contrast, there was no change in the expression levels of unrelated genes including GAPDH and β-actin ($P = 0.75$ and 0.27, respectively, data not shown). The transgenic mice showed no remarkable phenotype during development. The adult mice exhibited mild fatty liver (Fig. 1B and C) and female infertility (data not shown), which were also observed in SOD1-null mice [15,16]. These findings indicate that the phenotype of the anti-SOD1 shRNA transgenic mice is similar to that of SOD1-null mice.

3.2. The siRNA-silencing efficiency differs among the tissues of the shRNA transgenic mice

We analyzed the siRNA-silencing efficiency in the various tissues of the shRNA transgenic mice. On Western blot analysis, we observed marked suppression of SOD1 protein in all the tissues examined (Fig. 2A). However, the siRNA-silencing efficiency was clearly different among the tissues; it was extremely high in the liver and skeletal muscle (>95%) and, in contrast, was relatively low in the central nervous system and lung (~80%) (Fig. 2A and B). The

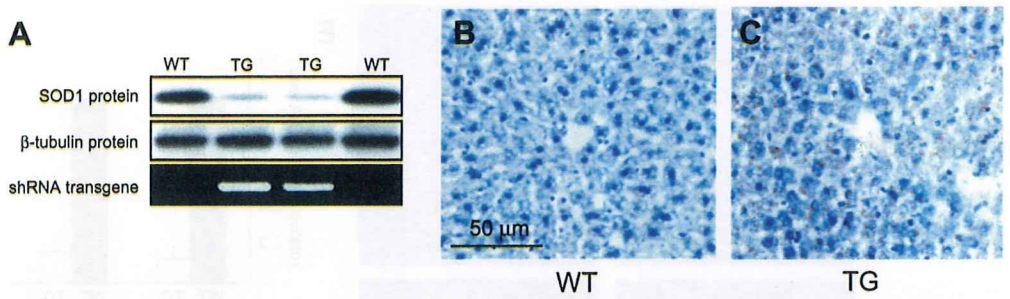

Fig. 1. Generation of anti-SOD1 shRNA transgenic mice. (A) Western blot analysis of SOD1 (upper) and β-tubulin (middle), and genomic PCR of transgene (lower) in the tails. Histological analysis in the liver of the wild-type littermates (B) and shRNA transgenic mice (C). The sections were stained with Sudan III. WT, age-matched wild-type littermates; TG, transgenic mice.

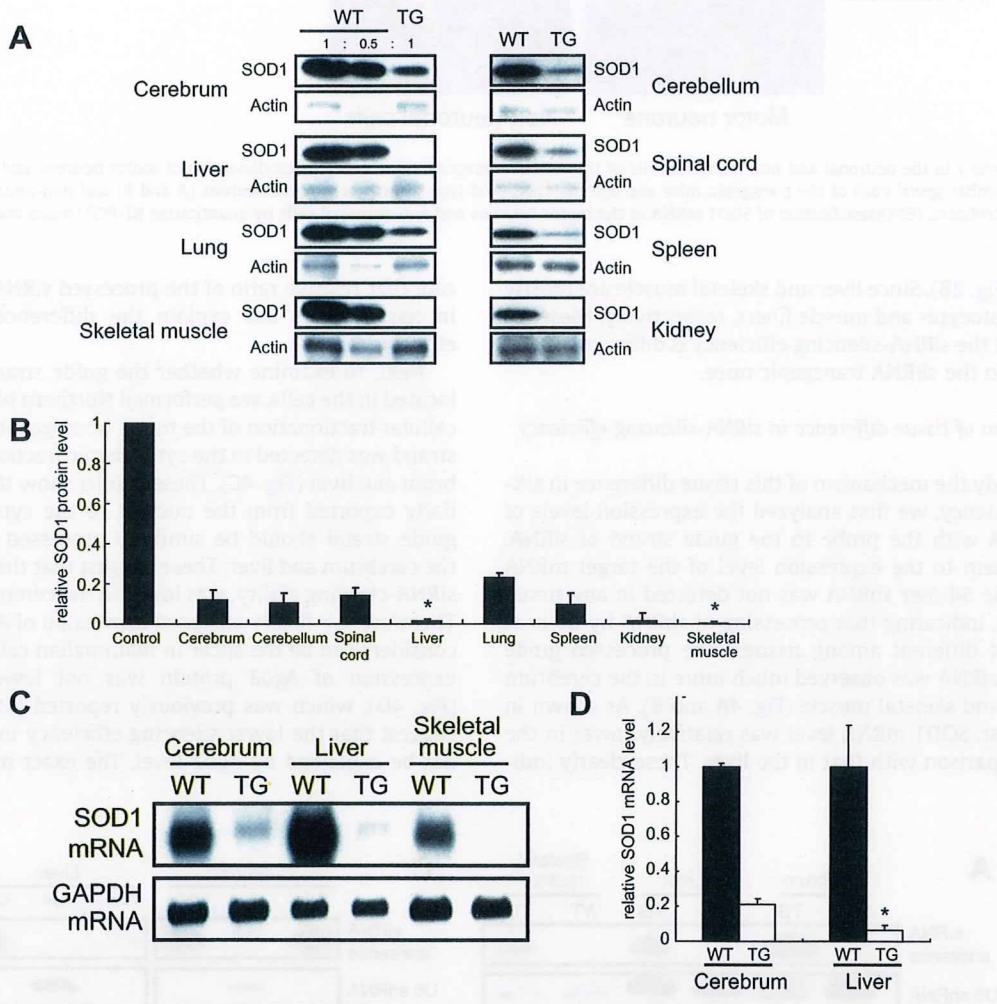

Fig. 2. Silencing efficiency in the various tissues of the shRNA transgenic mice. (A) SOD1 protein levels on Western blot analysis in the tissues of the transgenic mice. A half amounts of the wild-type samples are loaded in the middle lanes of left panel to show that the signals are not saturated. (B) Quantification of their band intensities. Values are the ratio to those of age-matched wild-type littermates (mean and S.D., $n = 3$, $^{*}P < 0.05$; significance compared to cerebrum). (C) SOD1 mRNA of the cerebrum, liver and skeletal muscle on Northern blot analysis. (D) Quantitative RT-PCR of SOD1 mRNA in the cerebrum and liver. Values are the ratio to age-matched wild-type littermates (mean and S.D., $n = 3$, $^{*}P < 0.05$; significance compared to cerebrum).

difference was also confirmed on RNA level by Northern blot analysis (Fig. 2C) and quantitative RT-PCR (Fig. 2D).

3.3. The siRNA-silencing efficiency in neuronal cells is relatively lower than those in hepatocytes and muscle fibers

Because central nervous system is composed of heterogenous cell populations, we sought to evaluate the siRNA-silencing efficiency in neuronal and non-neuronal cells using laser microdissection method. The motor neurons and non-neuronal cells were isolated from the ventral horn of the lumbar spinal cords in the shRNA transgenic mice or wild-type littermates (Fig. 3A–D), and SOD1 mRNA levels were quantified by quantitative RT-PCR. The silencing efficiency in the motor neurons was approximately 80% which was similar to the non-neuronal cells (Fig. 3E) and the whole spinal cord tissue (Fig. 2B), and was less than those in the liver and

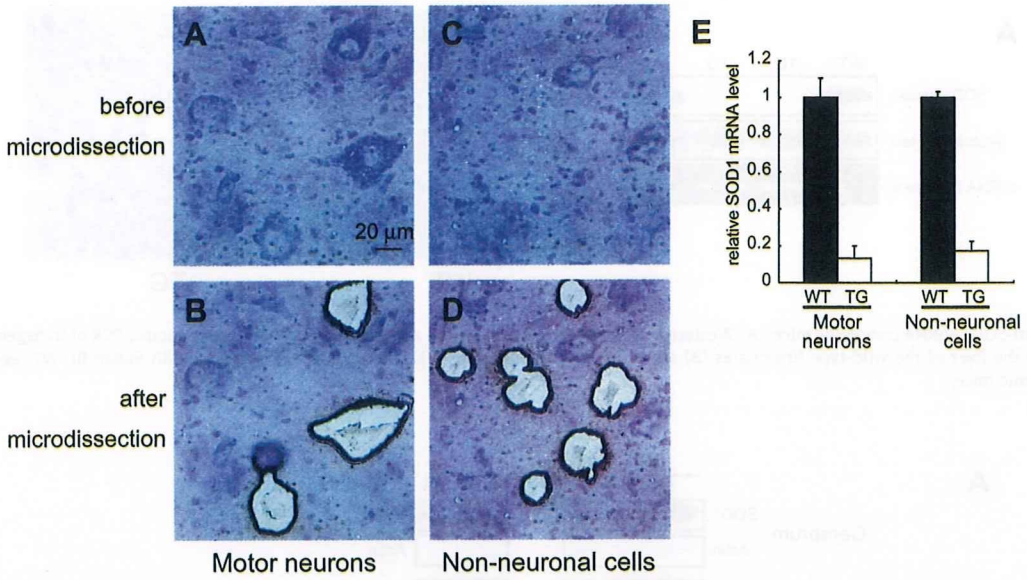

Fig. 3. Silencing efficiency in the neuronal and non-neuronal cells of the shRNA transgenic mice. (A–D) Microdissection of motor neurons and non-neuronal cells in the ventral horn of the lumbar spinal cord of the transgenic mice and age-matched wild-type littermates. Motor neurons (A and B) and non-neuronal cells (C and D) were dissected by laser microbeam. (E) Quantification of SOD1 mRNA in the motor neurons and non-neuronal cells by quantitative RT-PCR (mean and S.D., $n = 3$).

skeletal muscle (Fig. 2B). Since liver and skeletal muscle are mostly composed of hepatocytes and muscle fibers, respectively, these results indicate that the siRNA-silencing efficiency is different among cell populations in the shRNA transgenic mice.

3.4. The mechanism of tissue difference in siRNA-silencing efficiency

In order to study the mechanism of this tissue difference in siRNA-silencing efficiency, we first analyzed the expression levels of shRNA and siRNA with the probe to the guide strand of siRNA, and compared them to the expression level of the target mRNA in each tissue. The 54 mer shRNA was not detected in any tissue (data not shown), indicating that processing of shRNA by Dicer is excellent and not different among tissues. The processed guide strand of 21 mer siRNA was observed much more in the cerebrum than in the liver and skeletal muscle (Fig. 4A and B). As shown in Fig. 2C, in contrast, SOD1 mRNA level was relatively lower in the cerebrum in comparison with that in the liver. These clearly indicate that relative ratio of the processed siRNA to the target mRNA in tissues does not explain the difference in siRNA-silencing efficiency.

Next, to examine whether the guide strand of siRNA properly located in the cells, we performed Northern blot analysis after subcellular fractionation of the tissue homogenates. Most of the guide strand was detected in the cytoplasmic fraction in both of the cerebrum and liver (Fig. 4C). These results show that the shRNA is similarly exported from the nucleus to the cytoplasm and that the guide strand should be similarly processed in the cytoplasm in the cerebrum and liver. These suggest that the slicer/RISC function, siRNA-cleaving ability, was lower in the cerebrum than in the liver. Therefore, we finally analyzed expression of Ago2 protein which is considered to be the slicer in mammalian cells [17]. However, the expression of Ago2 protein was not lower in the cerebrum (Fig. 4D), which was previously reported [18,19]. These findings suggest that the lower silencing efficiency in the cerebrum could not be explained by Ago2 level. The exact molecular mechanism

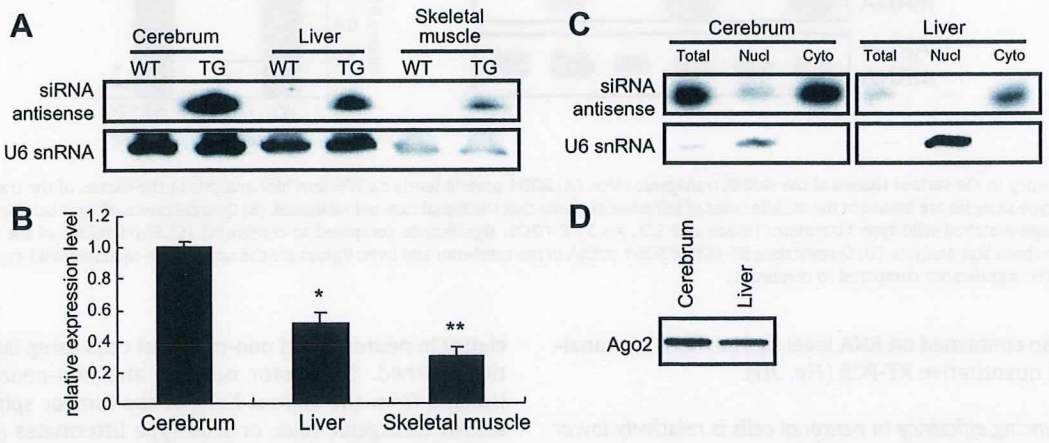

Fig. 4. The processing of shRNA/siRNA in the tissues of the transgenic mice. (A) Detection of siRNA guide strand in the cerebrum, liver and skeletal muscle on Northern blot analysis. (B) Quantification of their band intensity on Northern blot analysis. Values are the ratio to cerebrum (mean and S.D., $n = 3$, $^{*}P < 0.05$, $^{**}P < 0.01$; significance compared to cerebrum). (C) Subcellular localization of the siRNA guide strand in the cerebrum and liver. U6 snRNA is used as a marker of nuclear fraction. (D) Ago2 protein in the cerebrum and liver on Western blot analysis.

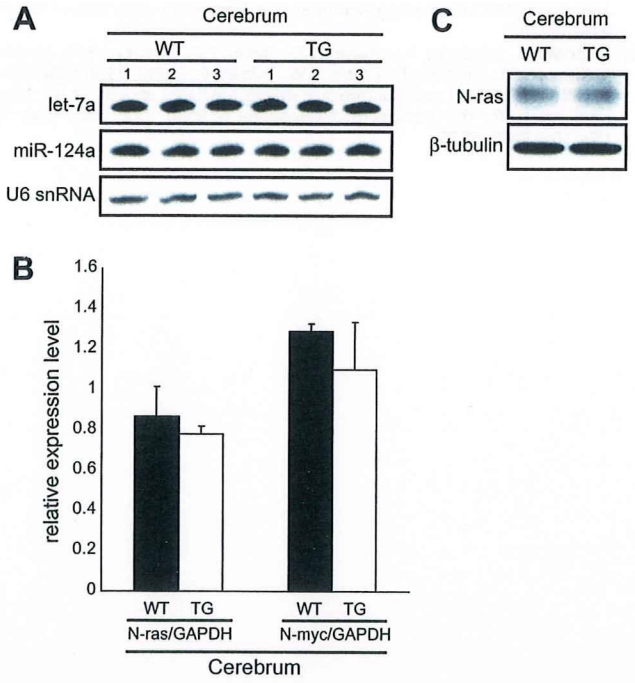

Fig. 5. Endogenous microRNA pathway in the shRNA transgenic mice. (A) Endogenous levels of miRNAs, let-7a (upper) and miR-124a (middle), in the cerebrum on Northern blot analysis. (B) Quantification of N-ras and N-myc levels, which are predicted as target genes of let-7a, in the cerebrum by quantitative RT-PCR (mean and S.D., $n = 3$). (C) N-ras protein in the cerebrum on Western blot analysis.

for the tissue difference in siRNA-silencing efficiency remains to be elucidated.

3.5. Endogenous miRNA pathway is not affected in the cerebrum of shRNA transgenic mice

To analyze whether competition between shRNA and miRNA occurred in the shRNA transgenic mice, we evaluated the expression levels of miRNAs and their target genes in the cerebrum of shRNA transgenic mice. There was no remarkable change in levels of let-7a and miR-124a on Northern blot analysis (Fig. 5A). Expression levels of N-ras and N-myc mRNAs, which were the predicted target genes of let-7a [20,21], were not altered on quantitative RT-PCR (Fig. 5B). Expression level of N-ras protein was not altered on Western blot analysis (Fig. 5C). These results clearly indicate that endogenous miRNA pathway is preserved in the shRNA transgenic mice.

The reproducibility of all results was confirmed by at least two experiments.

4. Discussion

We demonstrated the tissue difference in siRNA-silencing efficiency in the anti-SOD1 shRNA transgenic mice, but could not make clear the exact mechanism for the difference. However, the silencing effects in the tissues were generally good (>80%), and the anti-SOD1 shRNA transgenic mice could recapitulate the phenotype of fatty liver and female infertility as seen in SOD1-null mice [15,16].

Overexpression of shRNA from transgene did not induce apparent adverse effect including inhibition of endogenous miRNA pathway in our transgenic mice. It is of note that abundant shRNA/siRNA exogenously delivered by adeno-associated virus (AAV) vectors can cause drastic toxicity in the liver or brain possibly due to oversaturation of endogenous miRNA pathway [9,22]. The absence of the toxicity in the shRNA transgenic mice is probably due to its lower expression, because such a tissue toxicity is dependent on expression level of shRNA/siRNA [9,22]. Alternatively, there might be a difference in the processing pathways between shRNA expressed from transgene and that exogenously expressed by viral vector.

In conclusion, even with tissue difference in siRNA-silencing efficiency, endogenous miRNA pathway being well preserved, the transgenic RNAi approach is considered to be a useful method for analysis of gene function in vivo.

Acknowledgements

This work was supported by Grants from the Ministry of Health Labor and Welfare, Japan (#2212065, 2212070), the 21st Century COE Program on Brain Integration and its Disorders to Tokyo Medical and Dental University.

References

[1] Hannon, G.J. (2002) RNA interference. Nature 418, 244–251.
[2] Dykxhoorn, D.M. and Lieberman, J. (2005) The silent revolution: RNA interference as basic biology, research tool, and therapeutic. Annu. Rev. Med. 56, 401–423.
[3] Grimm, D. and Kay, M.A. (2007) Therapeutic application of RNAi: is mRNA targeting finally ready for prime time? J. Clin. Invest. 117, 3633–3641.
[4] Gao, X. and Zhang, P. (2007) Transgenic RNA interference in mice. Physiology 22, 161–166.
[5] Coumoul, X. and Deng, C.X. (2006) RNAi in mice: a promising approach to decipher gene functions in vivo. Biochimie 88, 637–643.
[6] Kunath, T., Gish, G., Lickert, H., Jones, N., Pawson, T. and Rossant, J. (2003) Transgenic RNA interference in ES cell-derived embryos recapitulates a genetic null phenotype. Nat. Biotechnol. 21, 559–561.
[7] Xia, X.G., Zhou, H., Samper, E., Melov, S. and Xu, Z. (2006) Pol II-expressed shRNA knocks down Sod2 gene expression and causes phenotypes of the gene knockout in mice. PLoS Genet. 2, e10.
[8] Rossi, J.J. (2008) Expression strategies for short hairpin RNA interference triggers. Hum. Gene Ther. 19, 313–317.
[9] Grimm, D., Streetz, K.L., Jopling, C.L., Storm, T.A., Pandey, K., Davis, C.R., Marion, P., Salazar, F. and Kay, M.A. (2006) Fatality in mice due to oversaturation of cellular microRNA/short hairpin RNA pathways. Nature 441, 537–541.
[10] Castanotto, D., Sakurai, K., Lingeman, R., Li, H., Shively, L., Aagaard, L., Soifer, H., Gatignol, A., Riggs, A. and Rossi, J.J. (2007) Combinatorial delivery of small interfering RNAs reduces RNAi efficacy by selective incorporation into RISC. Nucleic Acids Res. 35, 5154–5164.
[11] Saito, Y., Yokota, T., Mitani, T., Ito, K., Anzai, M., Miyagishi, M., Taira, K. and Mizusawa, H. (2005) Transgenic small interfering RNA halts amyotrophic lateral sclerosis in a mouse model. J. Biol. Chem. 280, 42826–42830.
[12] Yokota, T., Miyagishi, M., Hino, T., Matsumura, R., Tasinato, A., Urushitani, M., Rao, R.V., Takahashi, R., Bredesen, D.E., Taira, K. and Mizusawa, H. (2004) siRNA-based inhibition specific for mutant SOD1 with single nucleotide alternation in familial ALS, compared with ribozyme and DNA enzyme. Biochem. Biophys. Res. Commun. 314, 283–291.
[13] Ando, Y., Liang, Y., Ishigaki, S., Niwa, J., Jiang, Y., Kobayashi, Y., Yamamoto, M., Doyu, M. and Sobue, G. (2003) Caspase-1 and -3 mRNAs are differentially upregulated in motor neurons and glial cells in mutant SOD1 transgenic mouse spinal cord: a study using laser microdissection and real-time RT-PCR. Neurochem. Res. 28, 839–846.
[14] Tateno, M., Sadakata, H., Tanaka, M., Itohara, S., Shin, R.M., Miura, M., Masuda, M., Aosaki, T., Urushitani, M., Misawa, H. and Takahashi, R. (2004) Calcium-permeable AMPA receptors promote misfolding of mutant SOD1 protein and development of amyotrophic lateral sclerosis in a transgenic mouse model. Hum. Mol. Genet. 13, 2183–2196.
[15] Uchiyama, S., Shimizu, T. and Shirasawa, T. (2006) CuZn-SOD deficiency causes ApoB degradation and induces hepatic lipid accumulation by impaired lipoprotein secretion in mice. J. Biol. Chem. 281, 31713–31719.
[16] Matzuk, M.M., Dionne, L., Guo, Q., Kumar, T.R. and Lebovitz, R.M. (1998) Ovarian function in superoxide dismutase 1 and 2 knockout mice. Endocrinology 139, 4008–4011.
[17] Meister, G., Landthaler, M., Patkaniowska, A., Dorsett, Y., Teng, G. and Tuschl, T. (2004) Human Argonaute2 mediates RNA cleavage targeted by miRNAs and siRNAs. Mol. Cell 15, 185–197.
[18] González-González, E., López-Casas, P.P. and del Mazo, J. (2008) The expression patterns of genes involved in the RNAi pathways are tissue-dependent and differ in the germ and somatic cells of mouse testis. Biochim. Biophys. Acta 1779, 306–311.
[19] Sago, N., Omi, K., Tamura, Y., Kunugi, H., Toyo-oka, T., Tokunaga, K. and Hohjoh, H. (2004) RNAi induction and activation in mammalian muscle cells

where Dicer and eIF2C translation initiation factors are barely expressed. Biochem. Biophys. Res. Commun. 319, 50–57.
[20] Johnson, S.M., Grosshans, H., Shingara, J., Byrom, M., Jarvis, R., Cheng, A., Labourier, E., Reinert, K.L., Brown, D. and Slack, F.J. (2005) RAS is regulated by the let-7 microRNA family. Cell 120, 635–647.
[21] Sampson, V.B., Rong, N.H., Han, J., Yang, Q., Aris, V., Soteropoulos, P., Petrelli, N.J., Dunn, S.P. and Krueger, L.J. (2007) MicroRNA let-7a down-regulates MYC and reverts MYC-induced growth in Burkitt lymphoma cells. Cancer Res. 67, 9762–9770.
[22] McBride, J.L., Boudreau, R.L., Harper, S.Q., Staber, P.D., Monteys, A.M., Martins, I., Gilmore, B.L., Burstein, H., Peluso, R.W., Polisky, B., Carter, B.J. and Davidson, B.L. (2008) Artificial miRNAs mitigate shRNA-mediated toxicity in the brain: implications for the therapeutic development of RNAi. Proc. Natl. Acad. Sci. USA 105, 5868–5873.

THE JOURNAL OF BIOLOGICAL CHEMISTRY VOL. 284, NO. 48, pp. 33400–33408, November 27, 2009

Depletion of Vitamin E Increases Amyloid β Accumulation by Decreasing Its Clearances from Brain and Blood in a Mouse Model of Alzheimer Disease*[S]

Received for publication, August 9, 2009 Published, JBC Papers in Press, August 13, 2009, DOI 10.1074/jbc.M109.054056

Yoichiro Nishida[‡], Shingo Ito[§], Sumio Ohtsuki[§], Naoki Yamamoto[¶], Tsubura Takahashi[‡], Nobuhisa Iwata[‖], Kou-ichi Jishage[**], Hiromi Yamada[‡], Hiroki Sasaguri[‡], Shigefumi Yokota[‡], Wenying Piao[‡], Hiroyuki Tomimitsu[‡], Takaomi C. Saido[‖], Katsuhiko Yanagisawa[¶], Tetsuya Terasaki[§], Hidehiro Mizusawa[‡], and Takanori Yokota[‡1]

From the [‡]Department of Neurology and Neurological Science, Graduate School, Tokyo Medical and Dental University, 1-5-45 Yushima, Bunkyo-ku, Tokyo 113-8519, the [§]Department of Molecular Biopharmacy and Genetics, Graduate School of Pharmaceutical Sciences, Tohoku University, Aoba, Aramaki, Aoba-ku, Sendai, Miyagi 980-8578, the [¶]National Institute for Longevity Sciences, National Center for Geriatrics and Gerontology, 36-3 Gengo, Morioka, Obu, Aichi 474-8522, the [‖]Laboratory for Proteolytic Neuroscience, RIKEN Brain Science Institute, 2-1 Hirosawa, Wako-shi, Saitama 351-0198, and the [**]Chugai Research Institute for Medical Science, Inc., Gotenba, Shizuoka 412-8513, Japan

Increased oxidative damage is a prominent and early feature in Alzheimer disease. We previously crossed Alzheimer disease transgenic (*APPsw*) model mice with α-tocopherol transfer protein knock-out (*Ttpa*$^{-/-}$) mice in which lipid peroxidation in the brain was significantly increased. The resulting double-mutant (*Ttpa*$^{-/-}$*APPsw*) mice showed increased amyloid β (Aβ) deposits in the brain, which was ameliorated with α-tocopherol supplementation. To investigate the mechanism of the increased Aβ accumulation, we here studied generation, degradation, aggregation, and efflux of Aβ in the mice. The clearance of intracerebral-microinjected ^{125}I-Aβ$_{1-40}$ from brain was decreased in *Ttpa*$^{-/-}$ mice to be compared with wild-type mice, whereas the generation of Aβ was not increased in *Ttpa*$^{-/-}$*APPsw* mice. The activity of an Aβ-degrading enzyme, neprilysin, did not decrease, but the expression level of insulin-degrading enzyme was markedly decreased in *Ttpa*$^{-/-}$ mouse brain. In contrast, Aβ aggregation was accelerated in *Ttpa*$^{-/-}$ mouse brains compared with wild-type brains, and well known molecules involved in Aβ transport from brain to blood, low density lipoprotein receptor-related protein-1 (LRP-1) and p-glycoprotein, were up-regulated in the small vascular fraction of *Ttpa*$^{-/-}$ mouse brains. Moreover, the disappearance of intravenously administered ^{125}I-Aβ$_{1-40}$ was decreased in *Ttpa*$^{-/-}$ mice with reduced translocation of LRP-1 in the hepatocytes. These results suggest that lipid peroxidation due to depletion of α-tocopherol impairs Aβ clearances from the brain and from the blood, possibly causing increased Aβ accumulation in *Ttpa*$^{-/-}$*APPsw* mouse brain and plasma.

The accumulation of amyloid β (Aβ)[2] is the primary pathological event driving neurodegeneration in Alzheimer disease (AD). Support of this hypothesis is based on genetic evidence from cases of familial AD with β-amyloid precursor protein (APP) or presenilin mutations and the remarkable effect of Aβ elimination by its vaccine on AD phenotype. The suggested mechanism for Aβ accumulation in sporadic AD includes elevated generation of Aβ due to increased β-secretase activity (1), decreased degradation of Aβ (2), and decreased efflux of Aβ from the brain to blood (3).

Increased oxidative stress of brain is a key feature of sporadic AD and manifests predominantly as lipid peroxidation (4). There are several lines of evidence suggesting that the AD brain displays extensive oxidative damage to various biological macromolecules, including lipids, proteins, and nucleic acids (5). Both Aβ level and lipid peroxidation in the brain are increased with disease progression of AD. However, the direct relationship between Aβ accumulation and lipid peroxidation is unclear (6).

Among natural isomers of vitamin E, α-tocopherol (α-Toc) has the most potent biological activity and is a major antioxidant that protects polyunsaturated fatty acids from peroxidation. Brain α-Toc content is maintained by α-tocopherol transfer protein (α-TTP), which transfers α-Toc from chylomicron to very low-density lipoprotein in the liver and transports α-Toc from blood to brain (7, 8). We have developed an α-tocopherol transfer protein knock-out (*Ttpa*$^{-/-}$) mouse that showed marked lipid peroxidation because of a lack of α-Toc in the brain and considered it as a model for chronic oxidative stress to the brain (7). In a *Ttpa*$^{-/-}$ mouse brain, two lipid peroxidation markers, thiobarbituric acid reactive substrates

* This work was supported in part by a grant for Research on Psychiatric and Neurological Disease and Mental Health from the Ministry of Health, Labor, and Welfare of Japan (to T. Y. and H. M.), a grant from the 21st Century COE Program on Brain Integration and Its Disorders to Tokyo Medical and Dental University (to Y. N., H. S., and H. M.), a grant from the Ministry of Education, Science, and Culture (to N. I., H. T., T. Y., and H. T.), and a grant of the SORST of Japan Science and Technology Agency (to S. O. and T. Terasaki).

[S] The on-line version of this article (available at http://www.jbc.org) contains supplemental Tables 1–3.

[1] To whom correspondence should be addressed. Tel.: 81-3-5803-5234; Fax: 81-3-5803-0169; E-mail: tak-yokota.nuro@tmd.ac.jp.

[2] The abbreviations used are: Aβ, amyloid β; AD, Alzheimer disease; APP, β-amyloid precursor protein; α-TTP, α-tocopherol transfer protein; PBS, phosphate-buffered saline; BBB, blood-brain barrier; LRP-1, lipoprotein receptor-related protein-1; Pgp, p-glycoprotein; GLUT-1, glucose transporter-1; TTR, transthyretin; BEI, brain efflux index; CLtot, total body clearance; α-Toc, α-tocopherol; TBS, Tris-buffered saline; PIPES, 1,4-piperazinediethanesulfonic acid; CHAPS, 3-[(3-cholamidopropyl)dimethylammonio]-1-propanesulfonic acid; IDE, insulin-degrading enzyme.

and 4-hydroxynonenal, were increased, and lipofuscin was massively accumulated (7). It is of note that the same markers were elevated in AD brains (9–11). We previously crossed the AD transgenic (*APPsw*) model mouse (Tg2576) with *Ttpa*$^{-/-}$ mouse, and the resulting double-mutant (*Ttpa*$^{-/-}$*APPsw*) mouse showed earlier and more severe cognitive dysfunction and had increased amyloid plaques in the brain by depletion of α-Toc (12). As a next step, we have studied the mechanism of how chronic lipid peroxidation increased Aβ deposits. The studies of the lifecycle of Aβ from its generation to its metabolism have received an extraordinary amount of attention in the field of AD research. Although the Aβ level in the brain is determined by the rate of Aβ generation and clearance in the brain, the clearance of Aβ from circulation is also important for the Aβ accumulation in the brain, because the Aβ levels in the brain and in the blood are held in equilibrium (3). Therefore, we evaluated the Aβ generation in the brain and its clearance from the brain and from the blood in *Ttpa*$^{-/-}$ mouse. We also measured the aggregation capacity of Aβ in the brain to evaluate the effect of oxidative stress on the accumulation of Aβ in the brain.

EXPERIMENTAL PROCEDURES

Animals

All experiments were approved by the Animal Experiment Committees of Tokyo Medical and Dental University. We used *Ttpa*$^{-/-}$ mice from a C57BL/6J background (7). We crossbred *Ttpa*$^{-/-}$ mice with *APPsw* transgene hemizygous mice (Tg2576 from a C57BL/6-SJL background, Taconic, Hudson, NY), which is an AD model that overexpresses a human APP_{695} with a double mutation (*APPsw*; K670N,M671L) (13). We then cross-bred *Ttpa*$^{+/-}$*APPsw* and *Ttpa*$^{+/-}$ to produce the *Ttpa*$^{-/-}$*APPsw* mice. Animals were screened for the presence of APPsw and α-TTP genes by PCR analysis of tail DNA. Complete elimination of α-Toc from the brain is achieved only when the deletion of α-TTP gene is combined with the dietary restriction, because a part of α-Toc taken up from the small intestine can enter the brain even without α-TTP (7). Furthermore, it is impossible to produce mice with α-Toc-deficient diet because supplementation of α-Toc is necessary for the maintenance of pregnancy (7). The dietary restriction of α-Toc after birth could not eliminate α-Toc from the brain of wild-type mice (7). Therefore, to study the effect of α-Toc depletion on AD phenotype, we fed the resulting double mutant (*Ttpa*$^{-/-}$*APPsw*) mice on α-Toc-deficient diet (Funabashi Farm, Chiba, Japan) and compared with the *APPsw* littermate mice on normal diet (36 mg of α-Toc/kg). To determine whether the differences in the phenotypes between *APPsw* mice and *Ttpa*$^{-/-}$*APPsw* mice are caused by the *Ttpa*$^{-/-}$ gene effect or α-Toc-deficient effect, we furthermore made a group of *Ttpa*$^{-/-}$*APPsw* mice that were fed on α-Toc-supplemented diet (750 mg of α-Toc/kg, Funabashi Farm). Details for these diets were previously described (7). All mice were housed in plastic cages, received food and water *ad libitum*, and were maintained on a 12/12-h light-dark cycle (lights on at 09:00, off at 21:00).

Aβ Quantitation in the Brain and Plasma

Three or four 18-month-old mice for each group were anesthetized with an intraperitoneal injection of pentobarbital (60 mg/kg). After blood was collected, they killed by transcardiac perfusion with 0.01 M phosphate-buffered saline (PBS), pH 7.4. The cerebral hemisphere was homogenized in 50 mM Tris-HCl buffer (TBS), pH 7.6, containing 150 mM NaCl and a protease inhibitor mixture (Complete, Roche Diagnostics) supplemented with 0.7 μg/ml pepstatin A (Peptide Institute, Osaka, Japan) with a Teflon glass homogenizer and centrifuged at 200,000 × *g* for 20 min at 4 °C. The supernatant was defined as the TBS-soluble fraction. The pellet was solubilized by sonication in 6 M guanidine-HCl buffer containing a protease inhibitor mixture. The solubilized pellet was centrifuged as before, after which the supernatant was diluted 12-fold to reduce the concentration of guanidine-HCl and used as the TBS-insoluble fraction (guanidine-extractable). The amounts of $Aβ_{1-40}$ and $Aβ_{1-42}$ in each fraction and plasma were assayed using commercially available human $Aβ_{1-40}$ and $Aβ_{1-42}$ sandwich enzyme-linked immunosorbent assay kits (BioSource International, Inc., Camarillo, CA).

Northern Blot Analysis

Three or four 18-month-old mice in each group were examined. Total RNA was extracted from the brain by TRIzol (Invitrogen). Total RNA (2.5 μg) was fractionated in a formaldehyde-agarose gel and transferred to a Nytran membrane (Schleicher & Schuell). The upper part of the membrane was hybridized with a purified PCR fragment corresponding to human APPsw cDNA (bases 981–1578). The lower part was hybridized with a probe specific for glyceraldehyde-3-phosphate dehydrogenase to confirm the quantity of loaded RNA. The signals were visualized with a Gene Images CDP-star detection kit (Amersham Biosciences).

Western Blot Analysis

C-terminal Fragments of APP-β, -α, and -γ/ε—Three or four 18-month-old mice in each group were examined. To analyze C-terminal fragments -β, -α, and -γ/ε, the cerebral hemisphere was homogenized with 50 mM TBS and centrifuged at 800 × *g* for 10 min at 4 °C. The supernatant was centrifuged at 200,000 × *g* for 28 min at 4 °C, and the resultant pellet was resuspended with 20 mM PIPES, pH 7.0, containing 140 mM KCl, 0.25 M sucrose, 5 mM EGTA, and a protease inhibitor mixture. Protein concentration was determined using a BCA protein assay kit (Pierce) and adjusted. After incubation of the suspension at 37 °C for 60 min, it was delipidized with chloroform:methanol (2:1) and chloroform:methanol:distilled water (1:2:0.8) sequentially to improve sensitivity. The resultant protein fraction was dried by evaporation and then solubilized with a sample buffer containing 9 M urea. Samples (20 μg) were separated by 16.5% SDS-polyacrylamide gel electrophoresis and transferred electrophoretically to nitrocellulose membranes (Schleicher & Schuell). The membranes were boiled in PBS for 3 min to improve sensitivity. The blot was probed with the rabbit polyclonal antibody against the C terminus of APP (A8717, Sigma) followed by the avidin-biotin-peroxidase complex (ABC) method (Vectastain ABC kits, Vector Laboratories,

Burlingame, CA). The immunoreactive band on the membrane was visualized with a Supersignal West Pico Chemiluminescence kit (Pierce).

Proteins to Transport Aβ across the Blood-Brain Barrier (BBB)—Three sets of three 8-month-old mice in each group were examined. The vascular fraction of small vessels was prepared from whole cerebrum using a modified method reported previously (14). Briefly, brains were homogenized in 10 mM PBS. After centrifugation at 800 × *g* for 5 min at 4 °C, the pellets were suspended with a dextran solution (M_r 70,000; 15% w/v, Sigma) and centrifuged at 4500 × *g* for 10 min at 4 °C. The pellets were washed by 10 mM PBS twice and resuspended with 5 mM PBS for 10 min. After centrifuging at 800 × *g* for 5 min, the final pellets of small vessels were resuspended by pipetting and vortexed in the homogenization buffer containing 10 mM TBS, pH 7.4, containing 1 mM EDTA, 150 mM NaCl, 4% CHAPS, 1 mM phenylmethylsulfonyl fluoride, and a protease-inhibitor mixture (Complete-Mini, Roche Diagnostics). The 4.5-μg samples were separated by 7.5 and 15% SDS-polyacrylamide mini-gel and transferred to a nitrocellulose membrane. The membrane was probed with mouse anti-low density lipoprotein receptor-related protein-1 (LRP-1) (β-chain specific, American Diagnostica Inc., Stamford, CT) or mouse anti-p-glycoprotein (Pgp) (C219, Signet, Dedham, MA) followed by sheep anti-mouse secondary antibody conjugated to horseradish peroxidase (Amersham Biosciences). Rabbit anti-brain-type glucose transporter-1 (GLUT-1) antibody (Alpha Diagnostic International, San Antonio, TX) with donkey anti-rabbit secondary antibody (Amersham Biosciences) was also used. Bands were visualized by using an ECL Plus Western blotting system (Amersham Biosciences).

Protein to Transport Aβ into the Liver—Three 8-month-old mice in each group were examined. To prepare the crude membrane fraction, liver was homogenized in hypotonic lysis buffer (10 mM Tris, 10 mM NaCl, 1.5 mM $MgCl_2$, pH 7.4) with 1 mM phenylmethylsulfonyl fluoride and a protease-inhibitor mixture (Complete-Mini). After centrifugation at 8000 × *g* for 10 min at 4 °C, the supernatant was centrifuged at 100,000 × *g* for 60 min at 4 °C. The pellet obtained was regarded as the crude membrane fraction. Furthermore, to prepare the plasma membrane fraction of the liver, this obtained pellet was resuspended in 10 mM HEPES, 250 mM sucrose, pH 7.4, and overlaid on 38% sucrose solution and then centrifuged at 100,000 × *g* for 40 min at 4 °C using a swing rotor (SW40Ti; Beckman, Fullerton, CA). The turbid layer was collected and centrifuged at 100,000 × *g* for 1 h at 4 °C, and the obtained pellet was defined as plasma membrane fraction. The 2.5-μg samples were separated with 7.5% SDS-polyacrylamide mini-gel and transferred electrophoretically to a nitrocellulose membrane. The membrane was probed with mouse anti-LRP-1, rabbit anti-cadherin (ab16505, Abcam, Cambridge, UK), or mouse anti-β-actin (A2228, Sigma) followed by sheep anti-mouse secondary antibody conjugated to horseradish peroxidase or a goat anti-rabbit antibody (Pierce), respectively. Bands were visualized by using an ECL Plus Western blotting system or a Supersignal West Femto Maximum Sensitivity kit (Pierce).

Aβ Ligand Proteins in the Plasma—Three or four 14-month-old mice in each group were examined. The collected plasma was diluted with saline, and the 0.10-μl anti-apolipoprotein E (apoE) or 0.40-μl anti-transthyretin (TTR) samples were separated with 15% SDS-polyacrylamide mini-gel and transferred electrophoretically to a polyvinylidene difluoride membrane (Bio-Rad). The membrane was probed with goat polyclonal anti-apoE (sc-6384, Santa Cruz Biotechnology, Inc., Santa Cruz, CA) or rabbit anti-TTR (Dako, Glostrup, Denmark) followed by donkey anti-goat secondary antibody conjugated to horseradish peroxidase (Santa Cruz Biotechnology) or donkey anti-rabbit antibody (Amersham Biosciences). Bands were visualized by using an ECL Plus Western blotting system.

Aβ Degrading Proteins in the Brain—Three or five 23-month-old mice in each group were examined. The cerebral hemisphere was homogenized in homogenization buffer (0.1 M Tris-HCl, pH 8.0, 0.15 M NaCl, 1 mg/ml leupeptin, and 1 mg/ml pepstatin A) and centrifuged at 500 × *g* for 5 min. Membranes were prepared by precipitation of the postnuclear supernatant at 100,000 × *g* for 60 min. The resulting pellet was subjected to protein extraction using 2% SDS by homogenization and posterior centrifugation at 100,000 × *g* for 60 min at 4 °C. The supernatant was used as a membrane fraction. Protein concentration was determined using a BCA protein assay kit, and the membrane fraction (2.5 μg) was separated by 7.5% SDS-polyacrylamide gel electrophoresis and transferred electrophoretically to polyvinylidene difluoride membrane. The blotted membrane was probed with rabbit polyclonal anti-insulin-degrading enzyme (IDE) (Calbiochem) or mouse anti-flotillin (BD Biosciences) followed by donkey anti-rabbit or sheep anti-mouse secondary antibody conjugated to horseradish peroxidase (Amersham Biosciences). Bands were visualized by using an ECL Plus Western blotting system.

β- and γ-Secretase Activities Measurement

The total activities of β- and γ-secretase present in the cerebrum of four 9-month-old mice were determined using secretase-kits (R&D Systems, Wiesbaden, Germany) (15). Secretase enzymatic activities were proportional to the fluorometric reaction, and the data were corrected by subtraction of background control (reactions in the absence of tissue).

Study of Aβ Efflux from the Brain at the BBB

In vivo brain elimination experiments were performed using intracerebral microinjection as described previously (16, 17). Four 2- or 14-month-old mice in each group were anesthetized intramuscularly with a mixture of ketamine (125 mg/kg) and xylazine (1.22 mg/kg), then mounted on a stereotaxic frame (SRS-6, Narishige, Tokyo, Japan) to hold the heads in position. Using a dental drill, a bore hole was made 3.8 mm lateral to the bregma. Then extracellular fluid buffer (122 mM NaCl, 25 mM $NaHCO_3$, 3 mM KCl, 1.4 mM $CaCl_2$, 1.2 mM $MgSO_4$, 0.4 mM K_2HPO_4, 10 mM D-glucose, and 10 mM HEPES, pH 7.4) containing 0.012 μCi of ^{125}I-Aβ_{1-40} and 0.12 μCi of [^{3}H]dextran was injected over a period of 1 min using a 5.0-μl microsyringe (Hamilton, Reno, NE) fitted with a fine needle at a depth of 2.5 mm from the surface of the scalp, *i.e.* in the secondary somatosensory cortex 2 (S2) region. The needle was left in this configuration for an additional 4 min to prevent reflux of the injected solution along the injection track before being slowly retracted.

At the designated times after microinjection, aliquots of cerebrospinal fluid were collected from the cisterna magna as reported previously (17). The whole brain was subsequently removed, and the left cerebrum, right cerebrum, and cerebellum were isolated and dissolved in 2.0 ml of 2 M NaOH at 60 °C for 1 h. The ^{125}I radioactivity of the samples was measured in a γ-counter (ART300, Aloka, Tokyo, Japan) for 3 min. The samples were then mixed with 14 ml of Hionic-fluor (Packard Instrument Co.), and ^{3}H radioactivity was measured in a liquid scintillation counter (TRI-CARB2050CA, Packard Instrument Co.) for 5 min. No radioactivity associated with this efflux transport process was detected in the contralateral cerebrum, cerebellum, or cerebrospinal fluid (data not shown), suggesting the operation of a selective efflux transport process across the BBB. The brain efflux index (BEI) was defined by the equation BEI % = (test substrate undergoing efflux at the BBB)/(test substrate injected into the brain) × 100, and the percentage of substrate remaining in the ipsilateral cerebrum was determined from 100 − BEI (%) = (amount of test substrate in the brain/amount of reference in the brain)/(amount of test substrate injected/amount of injected as a reference in the brain) × 100. The apparent elimination rate constant (k_e) was determined from the slope given by fitting a semilogarithmic plot of 100 − BEI *versus* time using the nonlinear least-squares regression analysis program MULTI (18).

^{125}I-Aβ$_{1-40}$ Plasma Pharmacokinetic Studies

Four or five 2- and 25-month-old mice in each group were anesthetized intramuscularly with a mixture of ketamine (125 mg/kg) and xylazine (1.22 mg/kg), and the jugular vein was isolated. Their body temperature was kept at 37 °C on a hot plate. Each mouse received a bolus intravenous injection of ^{125}I-Aβ$_{1-40}$ (5 μCi; 100 μl) into the jugular vein. Blood samples (30 μl) were collected from the tail vein by using a heparinized microcapillary at various intervals (1, 3, 5, 10, 15, 30, 60, 120, and 360 min) after the injection. The blood samples were centrifuged at 10,000 × *g* for 5 min at 4 °C, and the supernatant was obtained. To assess the integrity of the peptides, a plasma aliquot at each time point was cold-precipitated with 10% trichloroacetic acid in saline. After trichloroacetic acid precipitation, the precipitant was dissolved in 200 μl of 2 M NaOH at 55 °C for 10 min. The ^{125}I radioactivity of the samples was measured in a γ-counter (ART300) for 3 min.

The plasma concentration *versus* time data were analyzed by MOMENT (19) based on the model-independent moment analysis method (20). Briefly, the area under the plasma concentration-time curve (AUC) extrapolated to infinity was calculated the equation AUC = AUC_{0-360} + C_{360}/k_e, in which AUC_{0-360} is the area under the curve from time 0 to the time of the last plasma sample at 360 min calculated by the log-trapezoidal method, C_{360} is plasma concentration of the last plasma sample at 360 min, and k_e is the terminal elimination rate constant estimated from terminal points using the Akaike's Information Criterion-based method. The total body clearance (CLtot) was calculated by the equation CLtot = dose/AUC, where dose is the administered amount of ^{125}I-Aβ$_{1-40}$. The mean residence time (MRT) and the steady-state volume of distribution (Vdss) were calculated by MRT = AUMC/AUC and Vdss = CL·MRT, where AUMC is the total area under the first-moment time curve extrapolated to infinity.

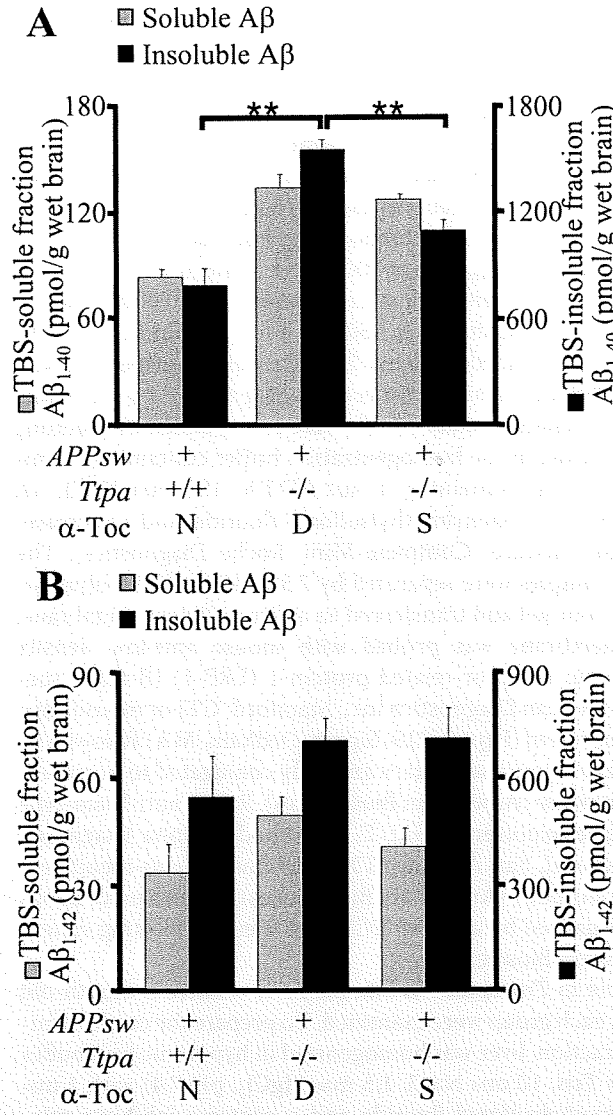

FIGURE 1. **The *Ttpa*$^{-/-}$*APPsw* mouse shows enhanced accumulation of Aβ in the brain.** *A* and *B*, cerebral Aβ$_{1-40}$ (*A*) and Aβ$_{1-42}$ (*B*) levels in 18-month-old mice. *Ttpa*$^{-/-}$*APPsw* mice showed increased level of Aβ$_{1-40}$ in the TBS-insoluble fraction of the brain homogenate and a similar tendency of increase of Aβ$_{1-40}$ and Aβ$_{1-42}$ in other fractions. This increase was partially ameliorated by α-Toc supplementation in the diet. *D*, α-Toc-deficient diet; *S*, α-Toc-supplemented diet; *N*, normal diet. **, $p < 0.01$.

Assay of Neprilysin-dependent Neutral Endopeptidase Activity

Four 4-month-old mice in each group were examined. Triton X-100-solubilized membrane fraction from brain was prepared to assay neutral endopeptidase activity as described previously (21). The neprilysin-dependent neutral endopeptidase activity was fluorometrically assayed using 0.1 mM succinyl-Ala-Ala-Phe-amidomethylcoumarin (Bachem, Bubendorf, Switzerland) as a substrate and determined from the fluorescence intensity (excitation, 390 nm; emission, 460 nm), based on the decrease in the rate of digestion caused by 0.1 μM thiorphan, a specific inhibitor of neprilysin.

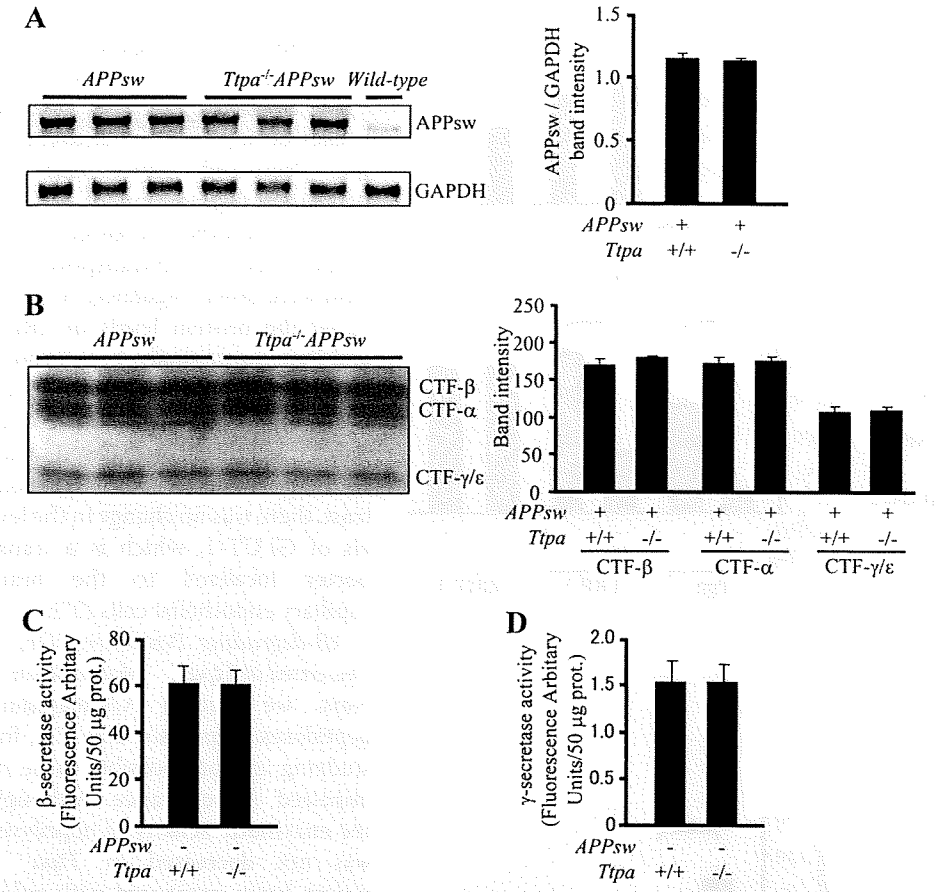

FIGURE 2. **α-Toc depletion does not increase APP expression nor β/γ-cleavages.** *A*, the human APPsw mRNA expression did not increase in the brains of *Ttpa*$^{-/-}$*APPsw* mice compared with *APPsw* mice. The band intensities normalized to the mouse glyceraldehyde-3-phosphate dehydrogenase (*GAPDH*) bands are shown in the *right panel*. *B*, protein levels of C-terminal fragments of APP-β, -α, and -γ/ε did not change in the brains of *Ttpa*$^{-/-}$*APPsw* mice compared with *APPsw* mice. Band intensities are shown in the *right panel*. *C* and *D*, the β (*C*)- and γ (*D*)-secretase activities did not increase in the brains of *Ttpa*$^{-/-}$ mice compared with wild-type mice.

Aβ Aggregation Study

Five 15-month-old *Ttpa*$^{-/-}$ mice and 10 age-matched wild-type mice were examined. Synaptosomes were prepared from mouse cerebrums as previously reported (22). Seed-free solutions of $A\beta_{1-40}$ were diluted with TBS. Aβ solutions at 50 μM were incubated at 37 °C with or without synaptosomes. Thioflavin T fluorescence intensities in the mixture incubated for 24 h were determined as previously described (23, 24).

Data Analysis

All data represent the average ± S.E. For multiple comparisons, single-factor analysis of variance followed by Fisher's protected least-significant-difference post hoc test was used. Results were considered statistically significant at $p < 0.05$.

RESULTS

Ttpa$^{-/-}$*APPsw Mouse Has an Enhanced Accumulation of Aβ in the Brain*—First, we biochemically studied the effect of α-Toc depletion on accumulation of Aβ. At 18 months, *Ttpa*$^{-/-}$*APPsw* mice showed markedly increased levels of $A\beta_{1-40}$ in the TBS-insoluble fraction of the brain homogenate and a similar tendency of increase of $A\beta_{1-40}$ and $A\beta_{1-42}$ in other fractions (Fig. 1, *A* and *B*). The *in vivo* accumulation of $A\beta_{1-40}$ was decreased when *Ttpa*$^{-/-}$*APPsw* mice were fed on the α-Toc-supplemented diet (Fig. 1*A*). An incomplete effect of α-Toc supplementation on accumulation of Aβ might be explained by the poor recruitment of supplemented α-Toc into the brain in *Ttpa*$^{-/-}$*APPsw* mice, because α-TTP in the brain transports α-Toc from blood to brain (7). This partial effect of α-Toc supplementation still could reduce accumulation of Aβ plaques (12).

APP Expression and β/γ Cleavages Are Not Increased—To examine the effect of α-Toc depletion on the metabolism of Aβ, we evaluated Aβ generation by measuring APP expression and secretase activities. The mRNA level of human APPsw in the brain did not increase in the brains of *Ttpa*$^{-/-}$*APPsw* mice compared with *APPsw* mice at 18 months of age (Fig. 2*A*). Moreover, protein levels of C-terminal fragments of APP-β, -α, and -γ/ε did not change in the brains of *Ttpa*$^{-/-}$*APPsw* mice compared with *APPsw* mice (Fig. 2*B*). This was supported by the *in vitro* results that β- and γ-secretase activities were not increased in the brains of 9-month-old *Ttpa*$^{-/-}$ mice (Fig. 2, *C* and *D*). These results indicate that the generation of Aβ in the brain of *Ttpa*$^{-/-}$*APPsw* mouse is not influenced by the depletion of α-Toc.

Aβ Clearance from the Brain Is Decreased in Ttpa$^{-/-}$ *Mice*—The increased Aβ accumulation without change of Aβ generation in *Ttpa*$^{-/-}$*APPsw* mouse brain led us to postulate that the increased Aβ accumulation by lipid peroxidation occurs through decreased Aβ clearance from the brain. Then we next directly studied Aβ clearance from the brain *in vivo* by using the BEI method (16, 17). We used *Ttpa*$^{-/-}$ mice in this experiment, because the injected ^{125}I-$A\beta_{1-40}$ should have been competed with endogenous Aβ, which accumulated in different degree in *Ttpa*$^{-/-}$*APPsw* and *APPsw* mouse brains, thereby complicating interpretation of the results. In contrast, *Ttpa*$^{-/-}$ mice have no detectable endogenous mouse Aβ in the brain. The ^{125}I-$A\beta_{1-40}$ was microinjected into the mouse cerebral cortex, and the remaining ^{125}I-$A\beta_{1-40}$ levels in the ipsilateral cerebrum were measured. The percentage of ^{125}I-$A\beta_{1-40}$ remaining at 60 min after injection was increased in 14-month-old *Ttpa*$^{-/-}$ mice compared with age-matched wild-type mice (Fig. 3*A*). The apparent elimination rate constant (k_e) was also markedly decreased because of α-Toc depletion (Fig. 3*B*). Although Aβ clearance decreases as a consequence of normal aging (25, 26), the reduction in k_e value evoked by α-Toc depletion (27.7%) was

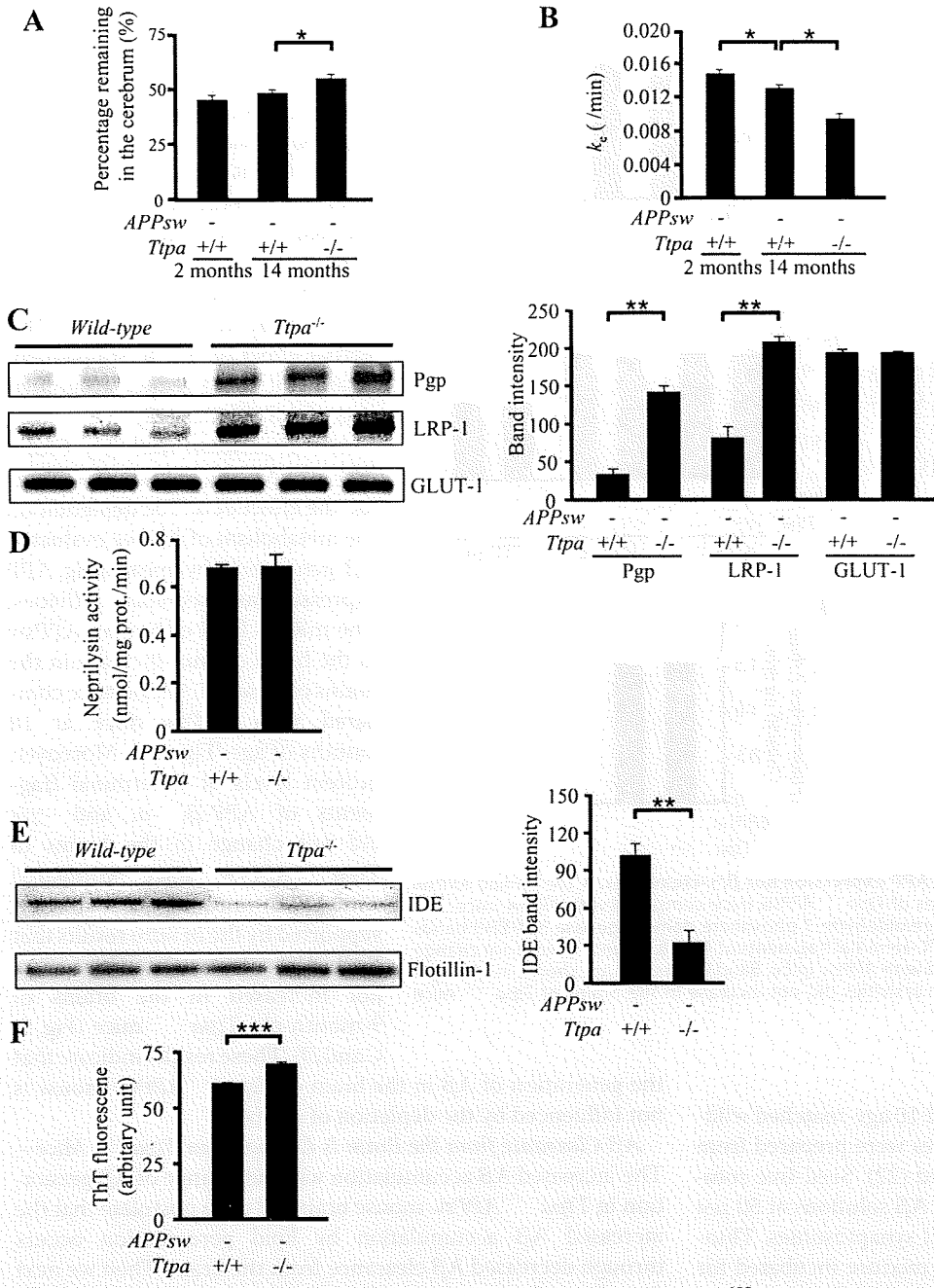

FIGURE 3. **α-Toc depletion decreases Aβ clearance.** *A*, the remaining percentage of ^{125}I-Aβ_{1-40} at 60 min was higher in 14-month-old *Ttpa*$^{-/-}$ mice than in age-matched wild-type mice. *B*, k_e was markedly decreased in *Ttpa*$^{-/-}$ mice. *C*, protein levels of LRP-1 and Pgp were increased in the brains of *Ttpa*$^{-/-}$ mice compared with wild-type mice, whereas levels of GLUT-1 were not changed between them. Band intensities are shown in the *right panel*. *D*, neprilysin-dependent endopeptidase activity did not decrease in *Ttpa*$^{-/-}$ mice compared with wild-type mice. *E*, protein levels of IDE were decreased in the brains of *Ttpa*$^{-/-}$ mice compared with wild-type mice. Band intensities are shown in the *right panel*. *F*, thioflavin T (*ThT*) fluorescence intensity in the incubation mixtures of synaptosomes with synthetic Aβ_{1-40} was increased in the brains of *Ttpa*$^{-/-}$ mice compared with wild-type mice. *, $p < 0.05$; **, $p < 0.01$; ***, $p < 0.0001$.

much greater than that by aging, as shown between 2 and 14 months of age (13.4%). One of the most likely pathologies influencing Aβ clearance is the compromised BBB by oxidative stress with vitamin E deficiency. However, there is no evidence of abnormal structures of endothelial cells or ischemic change on histological analysis of the *Ttpa*$^{-/-}$ mouse brains (data not shown).

Efflux Transporters for Aβ across the BBB Are Up-regulated in the Brain Capillary Endothelial Cells of Ttpa$^{-/-}$ *Mouse*—One of possible causes of impaired Aβ clearance is the decreased efflux and the decreased degradation of Aβ. To examine whether reported molecules involved in Aβ transport at the BBB were down-regulated, we measured the protein levels of LRP-1 and Pgp. Surprisingly, both protein levels in the small vascular fraction in the brains of *Ttpa*$^{-/-}$ mice were much increased compared with wild-type mice (Fig. 3*C*). In contrast, there was no change in the levels of GLUT-1, which is a transporter localized to the brain capillary endothelial cells (27).

Aβ-degrading Peptidase, IDE, Is Decreased in Ttpa$^{-/-}$ *Mouse Brain*—Next, we studied Aβ-degrading peptidases, neprilysin and IDE, for studying another possible cause of impaired Aβ clearance. Although the enzymatic activity of neprilysin was not decreased in *Ttpa*$^{-/-}$ mouse brain compared with wild-type mouse (Fig. 3*D*), expression level of IDE was markedly decreased in *Ttpa*$^{-/-}$ mouse brain (Fig. 3*E*). We, therefore, consider that an impaired degradation of Aβ in the brain because of decreased IDE is related with enhanced Aβ accumulation in *Ttpa*$^{-/-}$*APPsw* mouse brain.

Aβ Aggregation Is Accelerated in Ttpa$^{-/-}$ *Mouse Brains*—Moreover, we studied the effect of oxidative stress on Aβ aggregation capacity. The aggregation of Aβ_{1-40} in the presence of synaptosomes was measured by using thioflavin T fluorescence. The aggregation capacity was increased in brain homogenates of the *Ttpa*$^{-/-}$ mice compared with wild-type homogenates (Fig. 3*F*).

Ttpa$^{-/-}$*APPsw Mouse Has an Increased Level of Aβ in the Plasma as Well as in the Brain*—Furthermore, we measured the plasma levels of Aβ in *Ttpa*$^{-/-}$*APPsw* mouse. The 18-month-old *Ttpa*$^{-/-}$*APPsw* mice showed markedly increased levels of both plasma Aβ_{1-40} and Aβ_{1-42} (Fig. 4*A*). These accumulations of Aβ_{1-40} and Aβ_{1-42} were partially recovered when *Ttpa*$^{-/-}$*APPsw* mice were fed on the α-Toc-supplemented diet (Fig. 4*A*). In contrast, the Aβ-binding proteins in the plasma,

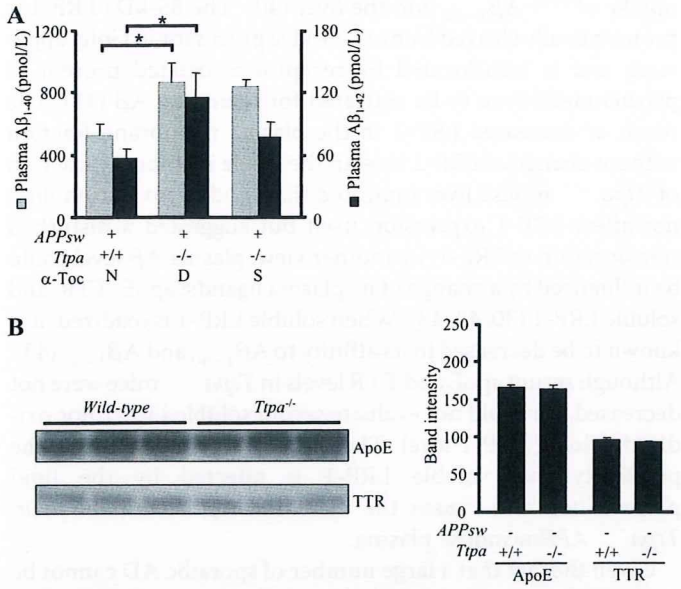

FIGURE 4. **The *Ttpa*$^{-/-}$*APPsw* mouse shows enhanced accumulation of Aβ in the plasma.** *A*, 18-month-old *Ttpa*$^{-/-}$*APPsw* mice showed increased levels of $A\beta_{1-40}$ and $A\beta_{1-42}$. This increase was partially ameliorated by α-Toc supplementation in the diet. *B*, protein levels of apoE and TTR were not changed in the plasma of *Ttpa*$^{-/-}$ mice compared with wild-type mice. Band intensities are shown in the *right panel*. *D*, α-Toc-deficient diet; *S*, α-Toc-supplemented diet; *N*, normal diet. *, $p < 0.05$.

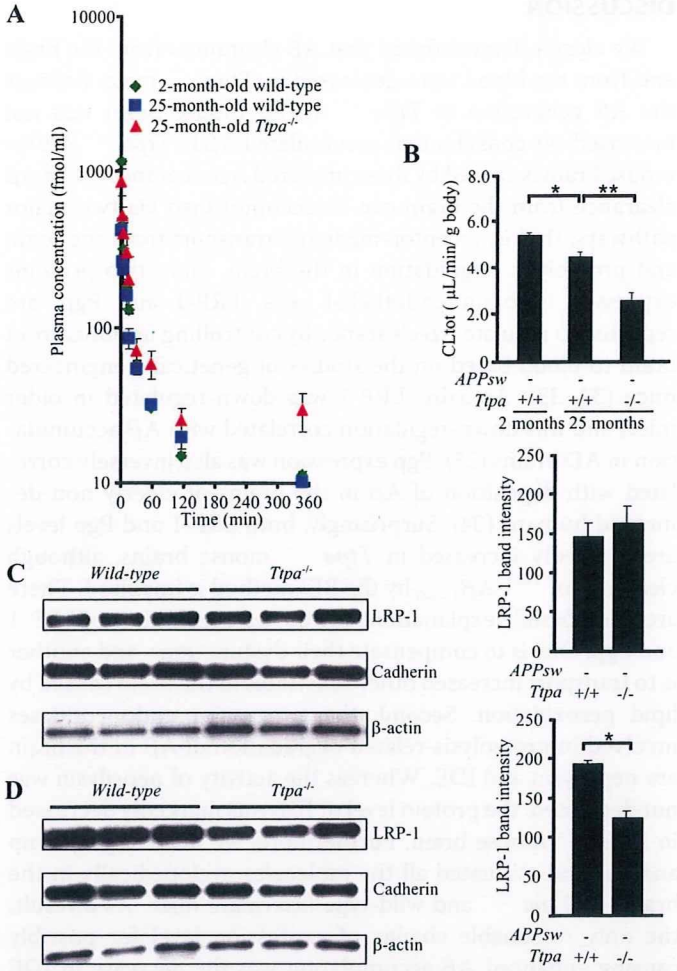

FIGURE 5. **α-Toc depletion decreases Aβ clearance from the plasma.** *A*, the remaining level of trichloroacetic acid-precipitable ^{125}I-$A\beta_{1-40}$ after its injection from the jugular vein was higher in 25-month-old *Ttpa*$^{-/-}$ mice than in wild-type mice. *B*, the total body clearance of ^{125}I-$A\beta_{1-40}$ was markedly decreased in *Ttpa*$^{-/-}$ mice compared with wild-type mice. *C* and *D*, the protein level of LRP-1 was decreased not in the crude membrane fraction of the liver of *Ttpa*$^{-/-}$ mice (*C*) but in the plasma membrane fraction (*D*) compared with wild-type mice. *, $p < 0.05$.

apoE, and TTR levels were not different between *Ttpa*$^{-/-}$ mice and wild-type mice (Fig. 4*B*).

Increased Aβ Accumulation in the Plasma Is also Caused by Impairment of Aβ Clearance from the Blood—The systemic clearance of Aβ should influence the levels of plasma Aβ. Therefore, the effect of *Ttpa* deficiency on systemic clearance of Aβ from the circulation was investigated *in vivo*. We also used *Ttpa*$^{-/-}$ in this experiment instead of *Ttpa*$^{-/-}$*APPsw* and *APPsw* mice, because the CLtot, a primary pharmacokinetic parameter that is a measure of the elimination efficiency of peripherally injected ^{125}I-$A\beta_{1-40}$, is known to decrease significantly in the presence of high plasma levels of $A\beta_{1-40}$ (28). Fig. 5*A* shows the plasma concentration-time profiles of trichloroacetic acid-precipitable ^{125}I-$A\beta_{1-40}$ after intravenous bolus administration in 2- and 25-month-old wild-type and 25-month-old *Ttpa*$^{-/-}$ mice. Plasma concentration of trichloroacetic acid-precipitable ^{125}I-$A\beta_{1-40}$ in 25-month-old *Ttpa*$^{-/-}$ mice was significantly greater at 1, 3, 60, and 360 min and substantially greater at all time points than that in 25-month-old wild-type mice (supplemental Table 1). As shown in supplemental Table 2, the AUC for *Ttpa*$^{-/-}$ mice was significantly greater than that for age-matched wild-type mice by 2.8-fold. To evaluate the systemic clearance more in detail, other pharmacokinetic parameters were determined and summarized in supplemental Table 2. In 25-month-old *Ttpa*$^{-/-}$ mice, CLtot and k_e (elimination rate constant) were significantly decreased by 41.2 and 51.7%, respectively, compared with those in age-matched wild-type mice (Fig. 5*B* and supplemental Table 2). The reduction in CLtot evoked by α-Toc depletion (41.2%) was much greater than that by aging, as shown between 2 and 25 months of age (14.1%) in model-independent moment analysis. The similar results were obtained in model dependent analysis as well (supplemental Table 2). These results demonstrated that systemic clearance was attenuated in 25-month-old *Ttpa*$^{-/-}$ mice, and the decrease in the systemic clearance is likely to be because of a decrease in the clearance from the liver, as the systemic clearance of Aβ has been reported to be mostly mediated by clearance from the liver (29, 30).

LRP-1 Is Down-regulated in the Plasma Membrane Fraction of the Liver in Ttpa$^{-/-}$ *Mice*—To examine whether the Aβ receptor was down-regulated in the liver for the cause of impaired Aβ clearance from the blood, we measured the protein level of LRP-1 in the crude and plasma membrane fractions of the liver, as LRP-1 translocates from Golgi apparatus to plasma membrane in their activation for transporting Aβ into the hepatocytes (31). The protein level of LRP-1 was unchanged in the crude membrane fraction but decreased in the plasma membrane fraction of *Ttpa*$^{-/-}$ mouse liver (Fig. 5, *C* and *D*). This inactivation of LRP-1 might explain the decreased clearance of Aβ from the blood, causing increased Aβ in *Ttpa*$^{-/-}$*APPsw* mouse plasma.

DISCUSSION

We clearly demonstrated that Aβ clearances from the brain and from the blood were decreased in *Ttpa*$^{-/-}$ mice. Because the Aβ generation in *Ttpa*$^{-/-}$*APPsw* mouse brain was not increased, we consider that accumulated Aβ in *Ttpa*$^{-/-}$*APPsw* mouse brain is caused by these impaired Aβ clearances. The Aβ clearance from the brain can be accomplished via two major pathways; that is, receptor-mediated transport from the brain and proteolytic degradation in the brain. First, two proteins expressed in brain endothelial cells, LRP-1 and Pgp, are reported to regulate Aβ clearance by controlling its efflux from brain to blood based on the studies of genetically engineered mice (32, 33). Actually, LRP-1 was down-regulated in older mice, and this down-regulation correlated with Aβ accumulation in AD brains (25). Pgp expression was also inversely correlated with deposition of Aβ in the brains of elderly non-demented humans (34). Surprisingly, both LRP-1 and Pgp levels are markedly increased in *Ttpa*$^{-/-}$ mouse brains, although clearance of ^{125}I-Aβ$_{1-40}$ by the BEI method is impaired. There are two possible explanations for the up-regulations of LRP-1 and Pgp. One is to compensate their dysfunctions, and another is to transport increased other substrates in the brain caused by lipid peroxidation. Second, the two major endopeptidases involved in proteolysis-related degradation of Aβ in the brain are neprilysin and IDE. Whereas the activity of neprilysin was not decreased, the protein level of IDE was markedly decreased in *Ttpa*$^{-/-}$ mouse brain. Furthermore, we made a gene chip analysis and evaluated all the molecules cyclopedically in the brains of *Ttpa*$^{-/-}$ and wild-type littermate mice. As a result, the only reasonable change of expression level for possibly causing enhanced Aβ accumulation was the decrease in IDE mRNA (supplemental Table 3, *A* and *B*). The homozygous deletion of IDE gene are known to show decreased Aβ degradation and increased accumulation of endogenous Aβ in the mouse brains (35, 36). Moreover, we previously confirmed that contribution of IDE to the clearance of microinjected ^{125}I-Aβ$_{1-40}$ in the BEI method could be 25.3% by the pre-administration of IDE inhibitors, bacitracin (26). Together, as one of molecular mechanisms of Aβ accumulation and impaired clearance of Aβ in *Ttpa*$^{-/-}$*APPsw* mouse brains, we think that degradation of Aβ was impaired by decreased expression of IDE. However, we cannot exclude the possibility of dysfunction of other proteins because of lipid peroxidation, which may contribute to abnormal Aβ metabolism.

There are reports that AD patients showed increased levels of peripherally circulating Aβ (37, 38). In *Ttpa*$^{-/-}$*APPsw* mice as well, plasma Aβ levels are proved to be markedly increased to be compared with *APPsw* mice. Significantly lowered clearance of injected ^{125}I-Aβ$_{1-40}$ from the *Ttpa*$^{-/-}$ mouse blood could explain the increased plasma Aβ in *Ttpa*$^{-/-}$*APPsw* mice. Although the excretion of Aβ through the kidney accounts only for a minute portion of Aβ in the blood (39), the liver is the major organ responsible for blood clearance of Aβ (29). We previously reported that LRP-1 in hepatocytes plays an important role to uptake plasma Aβ because mice with down-regulated LRP-1 by knock-out of receptor-associated protein or hydrodynamic injection of siRNA showed a much decreased uptake of ^{125}I-Aβ$_{1-40}$ into the liver (40). The 85-kDa LRP-1 is proteolytically cleaved from a 600-kDa precursor in Golgi apparatus and is translocated by receptor-associated protein to plasma membrane to be activated for bounding Aβ (41). The result of decreased LRP-1 in the plasma membrane fraction without change of LRP-1 level in the crude membrane fraction of *Ttpa*$^{-/-}$ mouse liver indicated that lipid peroxidation does not affect LRP-1 expression itself but suggested a disturbed translocation of LRP-1. In another view, plasma Aβ level could be influenced by a change of its plasma ligands; apoE, TTR, and soluble LRP-1 (30, 42, 43). When soluble LRP-1 is oxidized, it is known to be decreased in its affinity to Aβ$_{1-40}$ and Aβ$_{1-42}$ (43). Although serum apoE and TTR levels in *Ttpa*$^{-/-}$ mice were not decreased, we could not evaluate serum soluble LRP-1 nor oxidized soluble LRP-1 level. Therefore, we cannot exclude the possibility that soluble LRP-1 is affected by the lipid peroxidation and causes the increased Aβ accumulation in *Ttpa*$^{-/-}$*APPsw* mouse plasma.

Given the fact that a large number of sporadic AD cannot be explained by increased Aβ generation (3), better understanding of the molecular and genetic basis of the Aβ clearance mechanisms may hold at least in part the key for research of AD pathology. A strongest risk factor for AD is aging (44), and lipid peroxidation may be a major cause for aging of the brain (45). In these respects, our findings of increased accumulation and aggregation of Aβ with impaired clearance due to lipid peroxidation are new aspects of AD pathology. We hope that further investigation on the molecular mechanism of impaired Aβ clearance due to lipid peroxidation provides a novel diagnostic and therapeutic target of AD.

Acknowledgments—We thank Hiroyuki Arai, Mikio Shoji, Akihiko Nunomura, and Masaki Nishimura for invaluable suggestions and discussion and Iichirou Oonishi for assistance.

REFERENCES

1. Li, R., Lindholm, K., Yang, L. B., Yue, X., Citron, M., Yan, R., Beach, T., Sue, L., Sabbagh, M., Cai, H., Wong, P., Price, D., and Shen, Y. (2004) *Proc. Natl. Acad. Sci. U.S.A.* **101,** 3632–3637
2. Iwata, N., Higuchi, M., and Saido, T. C. (2005) *Pharmacol. Ther.* **108,** 129–148
3. Zlokovic, B. V. (2004) *J. Neurochem.* **89,** 807–811
4. Barnham, K. J., Masters, C. L., and Bush, A. I. (2004) *Nat. Rev. Drug Discov.* **3,** 205–214
5. Moreira, P. I., Smith, M. A., Zhu, X., Nunomura, A., Castellani, R. J., and Perry, G. (2005) *Ann. N.Y. Acad. Sci.* **1043,** 545–552
6. Andersen, J. K. (2004) *Nat. Med.* **10,** S18–25
7. Yokota, T., Igarashi, K., Uchihara, T., Jishage, K., Tomita, H., Inaba, A., Li, Y., Arita, M., Suzuki, H., Mizusawa, H., and Arai, H. (2001) *Proc. Natl. Acad. Sci. U.S.A.* **98,** 15185–15190
8. Traber, M. G., Burton, G. W., and Hamilton, R. L. (2004) *Ann. N.Y. Acad. Sci.* **1031,** 1–12
9. Dowson, J. H., Mountjoy, C. Q., Cairns, M. R., and Wilton-Cox, H. (1992) *Neurobiol Aging* **13,** 493–500
10. Lovell, M. A., Ehmann, W. D., Butler, S. M., and Markesbery, W. R. (1995) *Neurology* **45,** 1594–1601
11. Sayre, L. M., Zelasko, D. A., Harris, P. L., Perry, G., Salomon, R. G., and Smith, M. A. (1997) *J. Neurochem.* **68,** 2092–2097
12. Nishida, Y., Yokota, T., Takahashi, T., Uchihara, T., Jishage, K., and Mizusawa, H. (2006) *Biochem. Biophys. Res. Commun.* **350,** 530–536
13. Hsiao, K., Chapman, P., Nilsen, S., Eckman, C., Harigaya, Y., Younkin, S.,

Yang, F., and Cole, G. (1996) *Science* **274,** 99–102
14. Kanda, T., Yoshino, H., Ariga, T., Yamawaki, M., and Yu, R. K. (1994) *J. Cell Biol.* **126,** 235–246
15. Apelt, J., Bigl, M., Wunderlich, P., and Schliebs, R. (2004) *Int. J. Dev. Neurosci.* **22,** 475–484
16. Kakee, A., Terasaki, T., and Sugiyama, Y. (1996) *J. Pharmacol. Exp. Ther.* **277,** 1550–1559
17. Hino, T., Yokota, T., Ito, S., Nishina, K., Kang, Y. S., Mori, S., Hori, S., Kanda, T., Terasaki, T., and Mizusawa, H. (2006) *Biochem. Biophys. Res. Commun.* **340,** 263–267
18. Yamaoka, K., Tanigawara, Y., Nakagawa, T., and Uno, T. (1981) *J. Pharmacobiodyn.* **4,** 879–885
19. Tabata, K., Yamaoka, K., Kaibara, A., Suzuki, S., Terakawa, M., and Hata, T. (1999) *Xenobiol. Metabol. Dispos.* **14,** 286–293
20. Yamaoka, K., Nakagawa, T., and Uno, T. (1978) *J. Pharmacokinet. Biopharm.* **6,** 547–558
21. Ogawa, T., Kiryu-Seo, S., Tanaka, M., Konishi, H., Iwata, N., Saido, T., Watanabe, Y., and Kiyama, H. (2005) *J. Neurochem.* **95,** 1156–1166
22. Igbavboa, U., Avdulov, N. A., Schroeder, F., and Wood, W. G. (1996) *J. Neurochem.* **66,** 1717–1725
23. Naiki, H., and Gejyo, F. (1999) *Methods Enzymol.* **309,** 305–318
24. Hayashi, H., Kimura, N., Yamaguchi, H., Hasegawa, K., Yokoseki, T., Shibata, M., Yamamoto, N., Michikawa, M., Yoshikawa, Y., Terao, K., Matsuzaki, K., Lemere, C. A., Selkoe, D. J., Naiki, H., and Yanagisawa, K. (2004) *J. Neurosci.* **24,** 4894–4902
25. Shibata, M., Yamada, S., Kumar, S. R., Calero, M., Bading, J., Frangione, B., Holtzman, D. M., Miller, C. A., Strickland, D. K., Ghiso, J., and Zlokovic, B. V. (2000) *J. Clin. Invest.* **106,** 1489–1499
26. Shiiki, T., Ohtsuki, S., Kurihara, A., Naganuma, H., Nishimura, K., Tachikawa, M., Hosoya, K., and Terasaki, T. (2004) *J. Neurosci.* **24,** 9632–9637
27. Pardridge, W. M., Boado, R. J., and Farrell, C. R. (1990) *J. Biol. Chem.* **265,** 18035–18040
28. Kandimalla, K. K., Curran, G. L., Holasek, S. S., Gilles, E. J., Wengenack, T. M., and Poduslo, J. F. (2005) *J. Pharmacol. Exp. Ther.* **313,** 1370–1378
29. Ghiso, J., Shayo, M., Calero, M., Ng, D., Tomidokoro, Y., Gandy, S., Rostagno, A., and Frangione, B. (2004) *J. Biol. Chem.* **279,** 45897–45908
30. Hone, E., Martins, I. J., Fonte, J., and Martins, R. N. (2003) *J. Alzheimers Dis.* **5,** 1–8
31. Tamaki, C., Ohtsuki, S., and Terasaki, T. (2007) *Mol. Pharmacol.* **72,** 850–855
32. Van, Uden, E., Mallory, M., Veinbergs, I., Alford, M., Rockenstein, E., and Masliah, E. (2002) *J. Neurosci.* **22,** 9298–9304
33. Cirrito, J. R., Deane, R., Fagan, A. M., Spinner, M. L., Parsadanian, M., Finn, M. B., Jiang, H., Prior, J. L., Sagare, A., Bales, K. R., Paul, S. M., Zlokovic, B. V., Piwnica-Worms, D., and Holtzman, D. M. (2005) *J. Clin. Invest.* **115,** 3285–3290
34. Vogelgesang, S., Cascorbi, I., Schroeder, E., Pahnke, J., Kroemer, H. K., Siegmund, W., Kunert-Keil, C., Walker, L. C., and Warzok, R. W. (2002) *Pharmacogenetics* **12,** 535–541
35. Farris, W., Mansourian, S., Chang, Y., Lindsley, L., Eckman, E. A., Frosch, M. P., Eckman, C. B., Tanzi, R. E., Selkoe, D. J., and Guenette, S. (2003) *Proc. Natl. Acad. Sci. U.S.A.* **100,** 4162–4167
36. Miller, B. C., Eckman, E. A., Sambamurti, K., Dobbs, N., Chow, K. M., Eckman, C. B., Hersh, L. B., and Thiele, D. L. (2003) *Proc. Natl. Acad. Sci. U.S.A.* **100,** 6221–6226
37. Kuo, Y. M., Emmerling, M. R., Lampert, H. C., Hempelman, S. R., Kokjohn, T. A., Woods, A. S., Cotter, R. J., and Roher, A. E. (1999) *Biochem. Biophys. Res. Commun.* **257,** 787–791
38. Matsubara, E., Ghiso, J., Frangione, B., Amari, M., Tomidokoro, Y., Ikeda, Y., Harigaya, Y., Okamoto, K., and Shoji, M. (1999) *Ann. Neurol.* **45,** 537–541
39. Ghiso, J., Calero, M., Matsubara, E., Governale, S., Chuba, J., Beavis, R., Wisniewski, T., and Frangione, B. (1997) *FEBS Lett.* **408,** 105–108
40. Tamaki, C., Ohtsuki, S., Iwatsubo, T., Hashimoto, T., Yamada, K., Yabuki, C., and Terasaki, T. (2006) *Pharm. Res.* **23,** 1407–1416
41. Willnow, T. E., Armstrong, S. A., Hammer, R. E., and Herz, J. (1995) *Proc. Natl. Acad. Sci. U.S.A.* **92,** 4537–4541
42. Matsubara, E., Sekijima, Y., Tokuda, T., Urakami, K., Amari, M., Shizuka-Ikeda, M., Tomidokoro, Y., Ikeda, M., Kawarabayashi, T., Harigaya, Y., Ikeda, S., Murakami, T., Abe, K., Otomo, E., Hirai, S., Frangione, B., Ghiso, J., and Shoji, M. (2004) *Neurobiol. Aging* **25,** 833–841
43. Sagare, A., Deane, R., Bell, R. D., Johnson, B., Hamm, K., Pendu, R., Marky, A., Lenting, P. J., Wu, Z., Zarcone, T., Goate, A., Mayo, K., Perlmutter, D., Coma, M., Zhong, Z., and Zlokovic, B. V. (2007) *Nat. Med.* **13,** 1029–1031
44. Katzman, R., and Saitoh, T. (1991) *FASEB J.* **5,** 278–286
45. Sohal, R. S., and Weindruch, R. (1996) *Science* **273,** 59–63

THE JOURNAL OF BIOLOGICAL CHEMISTRY VOL. 284, NO. 45, pp. 31291–31302, November 6, 2009

Dynein Dysfunction Induces Endocytic Pathology Accompanied by an Increase in Rab GTPases

A POTENTIAL MECHANISM UNDERLYING AGE-DEPENDENT ENDOCYTIC DYSFUNCTION[*][S]

Received for publication, April 23, 2009, and in revised form, September 12, 2009 Published, JBC Papers in Press, September 15, 2009, DOI 10.1074/jbc.M109.012625

Nobuyuki Kimura[‡1], **Makoto Inoue**[§], **Sachi Okabayashi**[‡¶], **Fumiko Ono**[‡¶], **and Takayuki Negishi**[‖]

From the [‡]*Laboratory of Disease Control, Tsukuba Primate Research Center, National Institute of Biomedical Innovation, 1-1 Hachimandai, Tsukuba-shi, Ibaraki 305-0843,* [§]*DNAVEC Research Inc., 1-25-11 Kannondai, Tsukuba-shi, Ibaraki 305-8421* [¶]*The Corporation for Production and Research of Laboratory Primates, 1 Hachimandai, Tsukuba-shi, Ibaraki 305-0843, and the* [‖]*Department of Chemistry and Biological Science, School of Science and Engineering, Aoyama Gakuin University, 5-10-1 Fuchinobe, Sagamihara-shi, Kanagawa 229-8558, Japan*

Growing evidence suggests that endocytic dysfunction is intimately involved in early stage Alzheimer disease pathology, such as the accumulation of β-amyloid precursor protein in enlarged early endosomes. However, it remains unclear how endocytic dysfunction is induced in an age-dependent manner. Cytoplasmic dynein, a microtubule-based motor protein, interacts with another microtubule-associated protein, dynactin. The resulting dynein-dynactin complex mediates minus end-directed vesicle transport, including endosome trafficking. We have previously shown that the interaction between dynein-dynactin complexes is clearly attenuated in aged monkey brains, suggesting that dynein-mediated transport dysfunction exists in aged brains. Our immunohistochemical analyses revealed that age-dependent endocytic pathology was accompanied by an increase in Rab GTPases in aged monkey brains. Here, we demonstrated that siRNA-induced dynein dysfunction reproduced the endocytic pathology accompanied by increased Rab GTPases seen in aged monkey brains and significantly disrupted exosome release. Moreover, it also resulted in endosomal β-amyloid precursor protein accumulation characterized by increased β-site cleavage. These findings suggest that dynein dysfunction may underlie age-dependent endocytic dysfunction via the up-regulation of Rab GTPases. In addition, this vicious circle may worsen endocytic dysfunction, ultimately leading to Alzheimer disease pathology.

The appearance of neuronal endocytic pathology before senile plaque deposition suggests that endocytic dysfunction is involved in early stage Alzheimer disease (AD)[2] pathology, such as the accumulation of β-amyloid precursor protein (APP) in enlarged early endosomes (1–4). β-Amyloid protein (Aβ), the major component of senile plaques, is produced from APP through sequential proteolytic cleavages by β- and γ-secretases, and such amyloidogenic cleavage, so-called β-site cleavage, of APP can occur through the endocytic pathway (1, 3). These findings suggest that endocytosis is involved in APP metabolism, and its dysfunction may lead to AD pathology. However, it remains unclear how endocytic dysfunction is induced in an age-dependent manner.

Cytoplasmic dynein is a microtubule-based motor protein required for minus end-directed axonal transport (5, 6). Dynactin, another microtubule-associated protein, binds to dynein intermediate chain (DIC) via its subunit, P150glued/dynactin (DYN) to form dynein-dynactin complexes that mediate minus end-directed vesicle transport, which includes endosome trafficking (7–12). We have previously shown that the interaction between DIC and DYN is clearly attenuated in aged monkey brains, suggesting that aging may impair dynein-mediated transport (13). Other studies also support this idea (14–17). Thus, in this study we investigated age-dependent endocytic pathology in cynomolgus monkey brains and tested our hypothesis of whether dysfunction of dynein causes endocytic dysfunction leading to AD pathology. Here, we demonstrated that siRNA-induced dysfunction of dynein reproduced the endocytic pathology and increased Rab GTPase levels observed in aged monkey brains. Moreover, dynein dysfunction also resulted in endosomal APP accumulation with a significant increase in β-site cleavage, representing early stage AD pathology.

EXPERIMENTAL PROCEDURES

Animals—Fourteen cynomolgus monkey (*Macaca fascicularis*) brains were used in this study. Of these, 6 brains were from young monkeys (ages 4 and 6 years), and 8 were from aged monkeys (ages 25, 26, 32, and 36 years). The frontal and temporal lobes of all the brains were used for immunohistochemical studies. The temporal lobes of eight cases (ages 4 years (n = 4), 25 years (n = 2), 26 years (n = 2)) were used for Western blot analyses.

All brains were obtained from the Tsukuba Primate Research Center, National Institute of Biomedical Innovation, Japan. All animals were housed in individual cages and maintained according to the National Institute of Biomedical Innovation

* This work was supported by a grant-in-aid from Comprehensive Research on Aging and Health, Ministry of Health, Labor, and Welfare, Japan.

[S] The on-line version of this article (available at http://www.jbc.org) contains a supplemental table and Figs. 1–3.

[1] To whom correspondence should be addressed. Fax: 81-29-837-0218; E-mail: kimura@nibio.go.jp.

[2] The abbreviations used are: AD, Alzheimer disease; APP, β-amyloid precursor protein; Aβ, β-amyloid protein; DIC, dynein intermediate chain; DYN, P150glued/dynactin; TGN, trans-Golgi network; TfR, transferrin receptor; DHC, dynein heavy chain; Flo-1, flotillin-1; sAPPα, secreted fragment of APP by α-secretase; sAPPβ, secreted fragment of APP by β-secretase; αCTF, C-terminal fragment of APP by α-secretase; βCTF, C-terminal fragment of APP by β-secretase; PBS, phosphate-buffered saline; siRNA, small interfering RNA; OA, okadaic acid.

rules and guidelines for experimental animal welfare. Three monkeys (ages 26 and 36 years) died naturally. The remaining animals were deeply anesthetized with pentobarbital.

Antibodies—In this study we used the following antibodies: mouse monoclonal anti-β-actin antibody (Sigma), mouse monoclonal anti-α-tubulin antibody (Santa Cruz Biotechnology, Santa Cruz, CA), mouse monoclonal anti-DIC antibody (Chemicon, Temecula, CA), mouse monoclonal anti-secreted fragment of APP by α-secretase (sAPPα) antibody (IBL, Gunma, Japan), mouse monoclonal anti-Aβ40 C-terminal 35–40 residue antibody (1A10; IBL), mouse monoclonal anti-rodent Aβ N-terminal antibody (14F1; IBL), mouse monoclonal anti-Rab5 antibody (Rab5m; Santa Cruz Biotechnology), mouse monoclonal anti-Rab11 antibody (Rab11m; Abcam, Cambridge, UK), mouse monoclonal anti-trans-Golgi network (TGN) antibody (Abcam), mouse monoclonal anti-Alix antibody (Santa Cruz Biotechnology), mouse monoclonal anti-transferrin receptor (TfR) antibody (Zymed Laboratories Inc., Carlsbad, CA), rabbit polyclonal anti-dynein heavy chain (DHC) antibody (Santa Cruz Biotechnology), rabbit polyclonal anti-DYN antibody (Santa Cruz Biotechnology), rabbit polyclonal anti-Rab5 antibody (Rab5r; Santa Cruz Biotechnology), rabbit polyclonal anti-Rab7 antibody (Rab7; Sigma), rabbit polyclonal anti-Rab11 antibody (Rab11r; Abcam), rabbit polyclonal anti-flotillin-1 (Flo-1) antibody (Santa Cruz Biotechnology), rabbit polyclonal anti-APP N-terminal antibody (APPn; IBL), rabbit polyclonal anti-APP C-terminal antibody (APPc; Zymed Laboratories Inc.), and rabbit polyclonal anti-secreted fragment of APP by β-secretase (sAPPβ) antibody (IBL). APPn predominantly recognizes full-length APP in Neuro2a cells (data not shown), and then it was used for immunocytochemistry. Because APPc can recognize both full-length APP and C-terminal fragment of APP by α-secretase (αCTF) or β-secretase (βCTF), it was used for Western blot analyses.

Immunohistochemistry—Immunostaining of monkey brains was performed as described elsewhere (18). Briefly, the brain samples were immersion-fixed with 4% paraformaldehyde, embedded in paraffin, and cut into 4-μm-thick sections. The sections were deparaffinized by pretreating with 0.5% periodic acid followed by autoclaving for 5 min at 121 °C, then incubated with a primary antibody solution overnight at 4 °C. In this study we used the following primary antibodies: anti-Rab5r (1:100), anti-Rab7 (1:200), and anti-Rab11r (1:200). After brief washes with buffer, the sections were sequentially incubated with biotinylated goat anti-mouse or anti-rabbit IgG then with a streptavidin-biotin-horseradish peroxidase complex (sABC kit; DAKO, Denmark). Immunoreactive elements were visualized by treating the sections with 3–3′ diaminobenzidine tetroxide (Dojin Kagaku, Japan). The sections were then counterstained with hematoxylin.

Subcellular Fractionation of Monkey Brains—Subcellular fractions from the temporal lobes of 8 monkeys were prepared at 0–4 °C as described by Tamai *et al.* (19). Briefly, sucrose solutions were prepared in a buffer containing 10 mM Tris-HCl (pH 7.6), 0.25 mM phenylmethylsulfonyl fluoride, and 1 mM EDTA. Brain tissue (~1.0 g) was homogenized in a glass homogenizer with 10 ml of 0.32 M sucrose solution and then centrifuged at 1000 × *g* for 10 min. The pellet (P1) was resuspended in 0.32 M sucrose, and this solution was layered over a discontinuous density gradient consisting of 1.2 and 0.85 M sucrose solutions. The suspension was centrifuged at 75,000 × *g* for 30 min in a Hitachi RPS-27 swing rotor to separate out P1 myelin and nuclei fractions. The supernatant (S1) from the P1 fraction was centrifuged at 13,000 × *g* for 15 min to yield the P2 fraction. The supernatant (S2) from the P2 fraction was centrifuged at 105000 × *g* for 60 min to obtain the microsomal (pellet) and cytosol (supernatant) fractions.

In this study we used the microsomal fraction for Western blot analyses. To normalize loading differences and confirm the purity of the fraction, we immunoblotted the fractions as described previously (20). Endoplasmic reticula and vesicles in the microsomal fraction were examined with mouse monoclonal anti-calnexin antibody (Santa Cruz Biotechnology; 1:500).

Western Blot Analyses for Age-related Changes in Rab GTPases in Monkey Brains—The proteins in the microsomal fractions were adjusted to 10 μg, and then each fraction was analyzed using SDS-PAGE and 12.5% acrylamide gels. Separated proteins were blotted onto polyvinylidene fluoride membranes (Immobilon P; Millipore, Bedford, MA). The membranes were blocked with 5% nonfat dried milk in 20 mM PBS (pH 7.0) and 0.1% Tween 20 for 1 h at room temperature and then incubated with primary antibodies overnight at 4 °C. In this study we used the following primary antibodies: anti-Rab5r (1:1000), anti-Rab7 (1:5000), and anti-Rab11r (1:5000). They were then incubated with either horseradish peroxidase-conjugated goat anti-mouse IgG or goat anti-rabbit IgG (Cell Signaling Technology, Danvers, MA) for 1 h at room temperature. Immunoreactive elements were visualized using enhanced chemiluminescence (Immobilon Western Detection Reagents; Millipore).

Cell Cultures—COS-7 cells were cultured in culture medium (Dulbecco's modified Eagle's medium with 10% fetal calf serum). Cells were plated at 2.0×10^4 cells/cm^2 onto 6-well plates coated with 0.01% poly-L-lysine (Wako, Osaka, Japan) for Western blot analyses and at 1.0×10^4 cells/cm^2 onto 2-well LAB-TEK chamber slides (Nalge Nunc, Rochester, NY) coated with 0.01% poly-L-lysine for immunocytochemistry. A neuronal cell line, mouse neuroblastoma Neuro2a cells, was also cultured in culture medium. Cells were plated at 1.5×10^4 cells/cm^2 onto 6-well plates coated with 0.01% poly-L-lysine for Western blot analyses at 1.5×10^4 cells/cm^2 onto 60-mm dishes coated with 0.01% poly-L-lysine for immunoprecipitation and at 1.0×10^4 cells/cm^2 onto 2-well LAB-TEK chamber slides (Nalge Nunc) coated with 0.01% poly-L-lysine for immunocytochemistry.

RNA Interference—For double-stranded RNA-mediated interference (RNAi) experiments we used the following short double-stranded RNA (siRNA) against primate-specific DHC (siDHC) and DYN (siDYN) for COS-7 cells and against mouse-specific DHC (siDHCm) for Neuro2a cells: siDHC, 5′-GGUGGGUGUACAUUACGAAUU-3′ (sense) and 5′-UUCGUAAUGUACACCCACCUG-3′ (antisense); siDYN, 5′-GGAGCGCUGUAUCGUAAGACC-3′ (sense) and 5′-UCUUACGAUACAGCGCUCCAG-3′ (antisense); siDHCm, 5′-GUAUCAGCACGGAGUUUUUGG-3′ (sense) and 5′-AAAAACUCCGUGC-

UGAUACUC-3′ (antisense). To avoid off-target effects, all siRNAs were carefully designed by Enhanced siDirect®. We also examined two different siRNAs for each target (see the supplemental table) and confirmed their knockdown-specific effects (data not shown). The control siRNA had a random sequence. RNAi experiments were performed by using siLentFect™ lipid reagent (Bio-Rad) according to the manufacturer's protocol.

Twenty-four or seventy-two hours after siRNA transfection, cells plated on 6-well plates were harvested in PBS and centrifuged to obtain cell pellets. The pellets were lysed in a sample buffer solution containing 62.5 mM Tris-HCl (pH 6.8), 2 mM EDTA, 0.5% Triton X-100, 2% SDS, and Complete Mini™ proteinase inhibitor mixture (Roche Applied Science) to extract total cellular proteins. Total proteins were adjusted to 10 μg and then subjected to SDS-PAGE by using 6% (DHC), 12.5% (other proteins), or 16% acrylamide gels (αCTF, βCTF, and Aβ). Separated proteins were blotted onto nitrocellulose membranes (Pall Life Sciences, Ann Arbor, MI) (Aβ) or polyvinylidene fluoride membranes (other proteins). Blotted nitrocellulose membranes were heated in boiling PBS for 5 min to enhance the signal (21) and then subjected to Western blot analyses as described above. We used the following primary antibodies: anti-β-actin (1:50000), anti-DHC (1:500), anti-DIC (1:20000), anti-DYN (1:2000), anti-Rab5r, anti-Rab7, anti-Rab11r, anti-APPc (1:1000), anti-sAPPα (1:1000), anti-sAPPβ (1:5000), and anti-Aβ40 C-terminal (1:500). We performed three independent experiments ($n = 6$ for each experimental group), duplicating each experiment.

Cells plated on chamber slides were fixed with 4% paraformaldehyde and then permeabilized with 0.01% (COS-7) or 0.1% (Neuro2a) Triton X-100 for 5 min at room temperature. After blocking with 3% bovine serum albumin, cells were incubated with primary antibodies overnight at 4 °C. Cells were then incubated with AlexaFluor 488-conjugated anti-mouse IgG and AlexaFluor 555-conjugated anti-rabbit IgG (Invitrogen) for 1 h at room temperature. All cells were examined with a Digital Eclipse C1 confocal microscope (NIKON, Kanagawa, Japan). For immunocytochemistry, we used the following primary antibodies: anti-DIC (1:10000), anti-Rab5m (1:1000), anti-Rab11m (1:200), anti-TGN (1:1000), anti-DYN (1:1000), anti-Rab5r (1:5000), anti-Rab7r (1:10000), anti-Rab11r (1:10000), and anti-APPn (1:2000). We performed three independent experiments.

Drug Treatments—COS-7 cells were treated with the following drugs at the indicated final concentrations: chloroquine (5 and 10 μM) and NH_4Cl (5 and 10 mM), both purchased from Wako. Neuro2a cells were cultured in serum-free culture medium containing 1% insulin-transferrin-selenium X supplement (Invitrogen) and then treated with okadaic acid (OA; 1 and 5 nM) (Calbiochem) dissolved in DMSO for 24 or 48 h. To wash and harvest cells treated with OA, we used PBS containing 10 mM NaF (Wako) and 2 mM Na_3VO_4 (Wako) to avoid dephosphorylation. Western blot analyses and immunocytochemistry were performed as described above. For Western blot analyses, we used the following primary antibodies: anti-β-actin, anti-DIC, anti-DYN, anti-Rab5r, anti-Rab7, and anti-Rab11r. We performed three independent experiments ($n = 6$ for each experimental group), duplicating each experiment. For immunocytochemistry, we used the following primary antibodies: anti-DIC, anti-α-tubulin (1:1000), anti-DYN, anti-Rab5r, anti-Rab7, and anti-Rab11r. We performed three independent experiments.

Semiquantitative Reverse Transcription-PCR—Primer sets were designed to recognize and amplify nucleotide sequences encoding mouse DHC (NM_030238), APP (NM_007471), and β-actin (NM_007393). cDNA sequences and/or the homologue(s) was identified using the BLAST (Basic Local Alignment Search Tool) computer program (National Center for Biotechnology Information, Bethesda, MD). Primers were designed using the Primer3 computer program (Whitehead Institute, Cambridge, MA).

Seventy-two hours after siRNA transfection, total cellular RNAs from Neuro2A cells were isolated using TRIzol reagent (Invitrogen). Single-stranded cDNAs were prepared via reverse transcription of a reaction mixture of total RNA (1 μg in 20 μl of reaction mixture), oligo$(dT)_{12-18}$ primers, and Superscript™II (Invitrogen). PCR amplification was performed using Thermo-Start™ (Thermo Fisher Scientific, Epsom, UK) and the following primers: DHC (+), 5′-CTCGGAAGCTTCGACAAAAC-3′; DHC (−), 5′-TCATCAGCTGTTTCCAGTGC-3′; APP (+), 5′-GGTTCTGGGCTGACAAACAT-3′; APP (−); 5′-GTGATGACAATCACGGTTGC-3′ β-actin (+); 5′-ATGGATGACGATATCGCTG-3′; β-actin (−), 5′-ATGAGGTAGTCTGTCAGGT-3′.

PCR products were electrophoresed in 1.5% agarose gels, and gels were subsequently stained with ethidium bromide. Densitometric analyses of gels were carried out with Quantity One Software (PDI Inc.). We performed three independent experiments ($n = 6$ for each experimental group), duplicating each experiment.

Immunoprecipitation—All steps were performed at 4 °C unless otherwise noted. For immunoprecipitation, we used recprotein G-Sepharose® 4B beads (Zymed Laboratories Inc.). Seventy-two hours after siRNA treatment, Neuro2a cell cultures (60 mm dish) were lysed in immunoprecipitation buffer solution containing 25 mM Tris-HCl (pH 8.0), 0.5% Triton X-100, 0.5% Nonidet P-40, and Complete Mini™ proteinase inhibitor mixture and then centrifuged at 105,000 × *g* for 15 min. The supernatant was recovered and then precleaned with Sepharose beads for 1 h. The precleaned supernatant containing 10 μg of proteins was incubated with anti-Aβ40 C-terminal antibody (1A10; 1 μg) or mouse IgG (Rockland Immunochemicals, Gilbertsville, PA) for 2 h. After immunoreactions, antibody-linked supernatant was incubated with precleaned beads for 1 h. The beads were washed with lysis buffer twice and then finally with Tris-buffered saline (50 mM Tris-HCl, pH 6.8). Protein was eluted from the beads with electrophoresis sample buffer and then analyzed using SDS-PAGE (16% acrylamide gels). Separated proteins were blotted onto nitrocellulose membranes. Blotted nitrocellulose membranes were heated in boiling PBS for 5 min to enhance the signal (21) and then subjected to Western blot analyses with anti-rodent Aβ N-terminal antibody (14F1; 1:2000). We performed five independent experiments.

Preparation of the Extracellular Membrane Fraction—Seventy-two hours after siRNA treatment, culture media from